Islamic Azad University
Mashhad Branch

Saadat and Stern / Iranian Journal of Earth Sciences 8 (2016) / 1-24

Distribution and geochemical variations among paleogene volcanic rocks from the north-central Lut block, eastern Iran

Saeed Saadat[1*], Charles R. Stern[2]

1. Department of Geology, Mashhad Branch, Islamic Azad University, Mashhad, Iran
2. Department of Geological Sciences, University of Colorado, Boulder, CO, USA

Received 11 October 2015; accepted 17 January 2016

Abstract

The Lut block in eastern Iran is a micro-continental block within the convergent orogen between the Arabian, Eurasian and Indian plates. Large areas of the north-central, eastern, and western Lut block are covered by volcanic rocks of Paleogene, Neogene and Quaternary age. Peak volcanic activity took place in the north-central part of the Lut block during the Eocene, and then dramatically decreased, becoming more restricted to the eastern and western margins of the block during the late Miocene and Quaternary. There is also significant variation in chemistry between the Paleogene igneous rocks from the north-central part compared to the Neogene and Quaternary volcanic rocks from the western and eastern margins of the Lut block. The Neogene and Quaternary olivine basalts, which were erupted along both margins of the Lut block, are similar in trace element chemistry to the average composition of oceanic island basalt. In contrast, the Paleogene volcanic units of the north-central Lut block, which include basalts through rhyolites, follow both calc-alkaline and alkaline trends. Low TiO_2 and high Ba/Nb and La/Nb ratios for both Paleogene basalts and andesitic samples from the north-central Lut block suggest affinities, at least for some of these samples, with convergent plate boundary arc magmas. LILE/HFSE ratios, interpreted as an indication of subduction signature, increase to the south-southwest of the central Lut block, where Neotethys oceanic crust was subducted beneath Iran in a northeastern direction from approximately Late Triassic to Late Oligocene time. We suggest that components derived from low angle subduction of this crust during the Mesozoic and early Tertiary were stored in the mantle lithosphere below the north-central Lut block until the Paleogene, when changing subduction geometry, associated with the collision of Arabia with Iran and the closing of Neotethys, caused hot asthenosphere to well up under the Lut block. This created the Eocene peak in volcanic activity, generating basalts from asthenospheric mixed with lithospheric melts, with both alkaline and calc-alkaline affinities. After this volcanism waned, becoming restricted during the Neogene to OIB-type alkaline basalts erupted through deep lithospheric structures along both the western and eastern margins of the Lut block.

Keywords: *Eastern Iran, Lut block, volcanism, basalts, subduction*

1. Introduction

The Lut block, a microcontinental block in eastern Iran (Fig. 1), occurs within the convergent orogen between the Arabian, Eurasian and Indian plates. Late Cretaceous to Neogene/Quaternary volcanic rocks, which cover a large area in this region, can provide a key for understanding the chemical and physical evolution of the continental crust and underlying mantle in the context of the complex tectonic evolution of this part of the Iranian Plateau which connects the Alpine and Himalayan orogenic systems. Magmatism in this continental collision area may involve contributions from subducted oceanic slabs, the asthenosphere, the sub-continental mantle lithosphere, and the continental crust. This paper presents information about the temporal distribution and geochemical variations of Paleogene and Neogene/ Quaternary volcanism from the north- central part of the Lut block with the goal of trying to better understand the petrogenesis of these igneous rocks and their relation with regional tectonic processes taking place during this time period.

*Corresponding author.
E-mail address (es): Saeed.Saadat@Colorado.edu

2. Background

2.1. Geotectonic setting

The Lut block is a micro-continental block which extends over 900 km in a north-south direction between latitudes 28° to 35°N, and is 250 km wide in an east-west direction between longitudes 57° to 61°E (Fig. 1). It is separated from the rest of the Iranian plateau on the east and west by major north-south structural zones. The overall uniformity of the Paleozoic platform strata and U–Pb geochronological data (Ramezani and Tucker 2003; Hassanzadeh et al. 2008; Horton et al. 2008) indicate that central–eastern

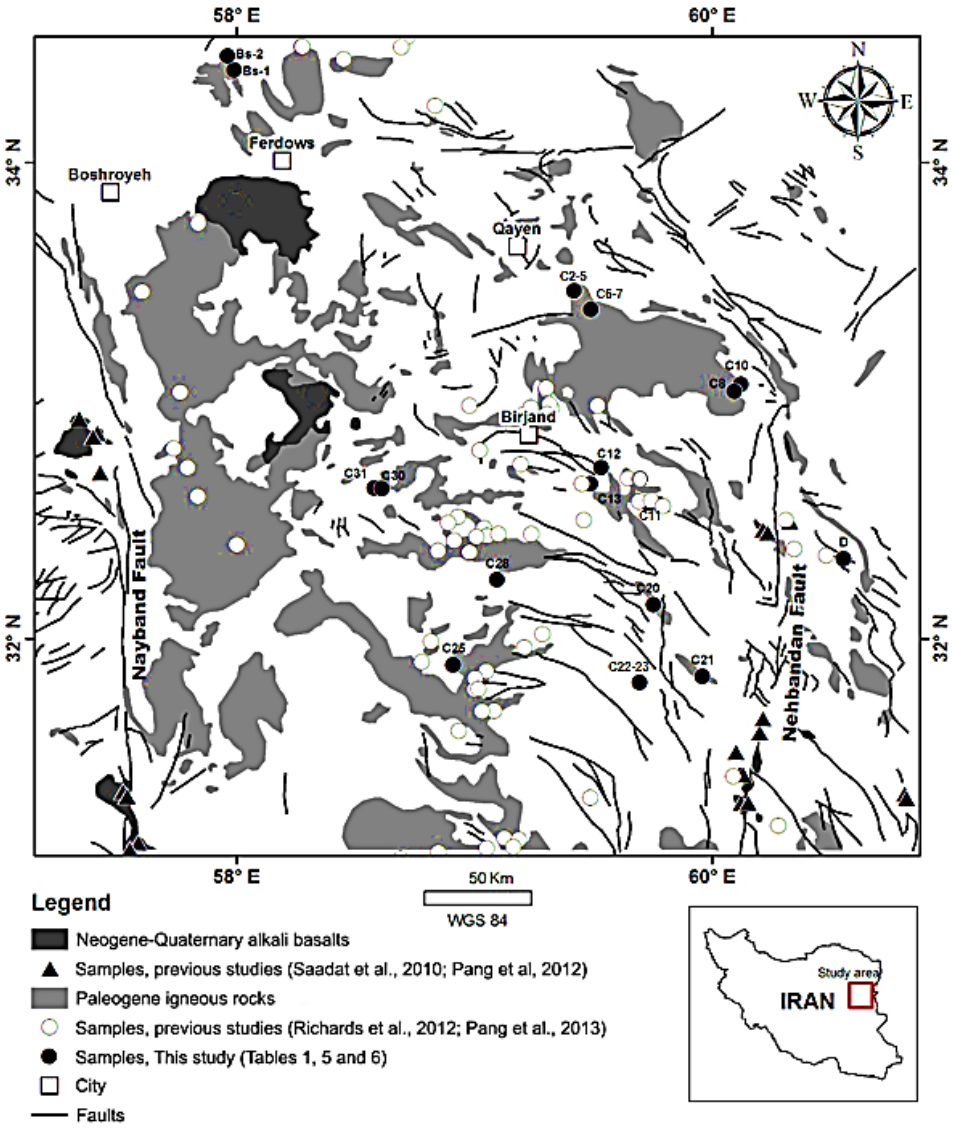

Fig. 1. Simplified distribution of volcanic rocks in the north-central Lut block with sample locations.

Iran, including the Lut block, was near Arabia and constituted a part of the Gondwanaland supercontinent during the early Paleozoic. From Late Precambrian until Late Paleozoic time, this region was separated from the Eurasian plate by the Hercynian Ocean called Paleotethys (Shahabpour 2005) and from Arabia by the Neotethys Ocean (Dercourt et al. 1993; Golonka et al. 1994; Sengör and Natalin, 1996).

The closure of Paleotethys by the northward motion of the central-eastern Iran and central Afghanistan micro-continents resulted in their welding with the Eurasian plate (Shahabpour 2005). Based on the zircon ages for the Shemshak sedimentary formation (Horton et al. 2008), the Iran–Eurasia collision must have happened during late Carnian–early Norian time (roughly 222–210 Ma). This is in agreement with the age proposed for the suture zone in the northeastern Iran by Alavi et al. (1997).

The Lut block is surrounded on the north, south and east by ophiolites and ophiolitic melanges formed as a result of closure of small Red Sea-type ocean basins during the Mesozoic (Takin 1972; McCall 1985; Shojaat et al. 2003). In the north, the eastern Iran domain is separated from the Alborz–Binaloud mountain range by the Sabzewar Basin (Kazmin 2010). To the west, in the Bafgh–Nain Zone, the ophiolitic melange separates eastern Iran from the Sanandaj–Sinjar Zone (Sengör 1990). Similar complexes, known as the Sistan suture zone, mark the Eastern Iranian Fold belt that extends from south to north between the eastern margin of the Lut block and the Afghan microcontinent (Delaloye and Desmons 1980; Saccani 2010; Zarrinkoub et al. 2012; Bröcker et al. 2013).

After the Iran–Eurasia collision, a new northward-dipping subduction zone developed along the northern margin of Neotethys (Golonka 2004). Subsequently,

the Arabian platform, which has been stable since Precambrian time and located adjacent to the Arabian shield, plunged beneath central Iran. This collision between Arabia and central Iran began sometime between the end of the Eocene and before the Miocene (e.g. Berberian and King 1981; Hatzfeld and Molnar 2010). Ages of early foreland basin fill in the Zagros fold-thrust belt also suggests that collision-related shortening was certainly underway by the late Oligocene–early Miocene (Fakhari et al. 2008; Horton et al. 2008). The northeastwards movement of the Arabian margin of the African–Arabian plate and the northeastward movement of India during the Cretaceous led to the narrowing of both western and eastern branches of Neotethys (Golonka et al. 1994). The evolution of the present central-eastern Iranian domain was controlled by a sequence of back-arc extensional and compressional cycles that were generated by the northeast-dipping Neotethys subduction (Bagheri and Stampfli 2008). Differences between the timing of subduction, the role of the trench pulling force, and the movement velocity of plates led to the development of several major strike-slip faults, which cut both continental and Jurassic–Cretaceous oceanic crust along the margins of the Lut block (Fig. 1; Jackson 1992; Kopp 1997; Golonka 2000; Saadat et al. 2010; Saadat and Stern 2012, 2014).

Wensink (1979, 1982), Wensink and Varekamp (1980), Soffel and Forster (1980), Davoudzadeh and Schmidt (1984), Bina et al. (1986), Soffel et al. (1996) and Saidi et al. (1997) also suggest the importance of rotations in central-eastern Iran at different scales (Besse et al. 1998). Compared to its present position the Lut block underwent a counter-clockwise rotation, relative to Eurasia, possibly during the Tertiary (Westphal et al. 1986; Soffel et al. 1996; Bagheri and Stampfli 2008) due to the collision of India and Afghanistan with Eurasia. According to paleomagnetic data presented by Soffel et al. (1996), the post Triassic counter clockwise rotation of the central–east Iranian block is about 135° with respect to Eurasia.

2.2. Geology of the Lut Block

The metamorphic basement of the north-central Lut block has not been dated and its age has remained poorly constrained. A large range, from Archean (Haghipour 1981) to Early Proterozoic (Nadimi 2007), Late Proterozoic (Davoudzadeh 1997; Samani et al. 1994) and Late Neoproterozoic to Early Cambrian (Hassanzadeh et al. 2008) crystallization ages for granitoids and granitic gneisses have been reported from the crystalline basement elsewhere in Iran. Sedimentary rocks in the Lut block are mainly younger than Permian and consist of shallow marine carbonates, shales and sandstones (Stöcklin et al. 1971). Continental Neogene sedimentary deposits, including upper Pliocene lacustrine silts, Quaternary sand dunes, salt flats, and alluvial fans cover large areas of the Lut block.

In the east and northeast of the Lut block, Cretaceous ultramafic and mafic ophiolitic rocks occur. These ophiolites are interpreted as remnants of Sistan oceanic lithosphere, a northwards projecting arm of the Neotethys Ocean (Tirrul et al. 1983; Bröcker et al. 2013; Angiboust et al. 2013; Zarrinkoub et al. 2012).

2.3. Magmatic activity

Based on limited geochronology data, magmatic activity in the Lut block started in the late Jurassic (Esmaiely et al. 2005; Tarkian et al. 1983) and continued into the Quaternary, forming a variety of volcanic and volcanoclastic rocks, as well as subvolcanic stocks. Sorkh-Kuh (Tarkian et al. 1984) and Shah-Kuh (Esmaiely et al. 2005), which are the most important granite complexes in the central Lut block, yield ages of 165-170 and 161-165 Ma, respectively. These granitoids rocks, and also Kuh-e-Bidmeshk plutonic complex, have similar compositions to continental volcanic arc granites (Tarkian et al. 1983), and could have been emplaced along an active continental margin setting.

Geochronology information indicates that the next episode of magmatism within the Lut block was during late Cretaceous. Two Rb/Sr dates by Baumann et al. (1982) yielded ages around 77 Ma for Bejestan S-type granitoid rocks located in the northwestern part of the Lut block. As pointed out by Jung et al. (1984), andesitic rocks around these intrusive rocks were affected by thermal metamorphism, which means the magmatic activity that produced these andesites must have started before the Bajestan granitoid was emplaced. Approximately 50 km to the southwest of Bejestan intrusive rocks, volcanic rocks of andesitic and dacitic composition are also exposed. The Rb-Sr age determination of these rocks corresponds to an age of 73 Ma (Jung et al. 1984). Further to southwest, between Ferdows and Dehuk, at the northeast edge of the Lut block, a medium-K dacite sample collected by Richards et al. (2012) from an area covered by volcanic and intrusive rocks yields an ages of 63.5 Ma.

Tertiary magmatic activity in the Lut block has been studied by many authors (Jung et al. 1984; Malekzadeh 2009; Arjmandzadeh et al. 2011; Karimpour et al. 2011; Richards et al. 2012; Pang et al. 2012, 2013; Kheirkhah et al. 2015). Jung et al. (1984) described Tertiary magmatic rocks in the northern part of the Lut block as including a wide compositional range from basaltic to rhyolitic, including both extrusive and intrusive forms. These andesite, dacite, and rhyodacite volcanic rocks were erupted together during the late Cretaceous to the early Neogene. Rhyolite ignimbrites in the northern part of the Lut block were erupted repeatedly during this volcanic activity. The oldest of these units is 60-63 Ma and the youngest units indicate K-Ar age around 31 Ma (Jung et al. 1984). Ar-Ar age

dating (Zarrinkoub et al. 2008) of one andesitic sample in central Lut block indicates a late Oligocene age (25.1 Ma). New 40Ar/39Ar age determination of Eocene–Oligocene magmatic rocks in the Sistan suture zone and central Lut block provided by Pang et al. (2013) indicate magmatism was active from the Middle Eocene (~46 Ma) to the Late Oligocene (~25 Ma) in this area. These results are consistent with a range of ages for basaltic samples between 43-15 Ma determined by Jung et al. (1984).

Neogene/Quaternary volcanic activity in the Lut block is mainly mafic in composition and located along the margins of the block (Saadat et al. 2010; Saadat and Stern 2011, 2012, 2014). Pang et al. (2012) indicate that this mafic volcanic activity began in the northern part of the eastern and western margin of the Lut block, at ~14 Ma and ~11 Ma, respectively, and by 1.6-2.2 Ma it had moved more toward the south (Walker et al. 2009; Pang et al. 2012, 2013; Chiu et al. 2013). Detail petrochemical characteristics of Neogene and Quaternary olivine basalts from the western and eastern margin of the Lut block are given by Saadat et al. (2010), Saadat and Stern (2011, 2012, 2014) and Pang et al. (2012).

3. Methods

Both standard petrographic thin sections and polished thin section for electron microprobe were prepared from samples (Table 1) of the central and eastern Lut block. Portions of these samples were also powdered for X-Ray fluorescence (XRF) spectrometry analysis for major elements, inductively coupled plasma mass spectrometer (ICP-MS) analysis for trace-elements, and also for determination of the Nd, Sr and Pb isotope compositions by solid source mass-spectrometry techniques described below.

Table 1. Location of samples from north-central Lut block.

Sample	Latitude	Longitude	Rock type	Sample	Latitude	Longitude	Rock type
D	32°20′30″	60°33′10″	Basalt	**C20-1**	32°08′36″	59°45′11″	Andesite
C2	33°27′37″	59°25′06″	Hawaiite	**C21**	31°50′33″	59°57′28″	Basalt
C3	33°27′37″	59°25′08″	Hawaiite	**C22-5**	31°49′00″	59°41′41″	Hawaiite
C4	33°27′35″	59°25′07″	Hawaiite	**C23-1**	31°49′00″	59°41′40″	Hawaiite
C5	33°27′34″	59°25′08″	Basalt	**C23-2**	31°49′00″	59°41′41″	Hawaiite
C6	33°27′09″	59°25′49″	Basalt	**C25**	31°53′28″	58°54′43″	Andesite
C7	33°27′09″	59°25′49″	Basalt	**C28**	32°14′51″	59°05′46″	Andesite
C8	33°02′23″	60°05′35″	Basalt	**C30-1**	32°37′53″	58°36′42″	trachyandesite
C10	33°04′06″	60°07′16″	Andesite	**C31-1**	32°38′01″	58°34′50″	Hawaiite
C11	32°34′03″	59°43′46″	Dacite	**C31-2**	32°38′01″	58°34′50″	phonolitic tephrite
C12	32°43′06″	59°31′57″	Hawaiite	**Bs-1**	34°23′19″	57°59′25″	Andesite
C13	32°39′04″	59°29′17″	trachyandesite	**Bs-2**	34°26′51″	57°57′43″	Basalt

The samples were examined in thin section, using standard techniques of optical mineralogy to determine their textures, mineral contents, and rock type. Following visual observation, description and photomicrography, selected thin sections were polished for electron microprobe to determine mineral compositions. This was done by using a 10 micron diamond polishing wheel, followed by a 6 micron polishing wheel and finally a 0.05 alumina powder on a felt pad. Minerals from polished sections were analyzed using the JEOL, JXA-8600 super probe, in the Laboratory for Environmental and Geological Science (University of Colorado at Boulder), with an electron gun accelerating voltage of 15 kV, current range from 17-24 nA and a one-micron diameter focused beam. Matrix correction was done by J Armstrong's ZAF correction program using natural mineral standards. Detailed discussion of using the electron microprobe as an analytical tool in geology is given by Reed (1996).

Rock samples were powdered for whole-rock geochemical analysis. A jaw crusher was used to pulverize samples, which were then powdered to 200 mesh with a tungsten carbide grinder. These rock powders were bottled and sent to the XRF laboratory in Ferdowsi University of Mashad (Iran), using Philips (X Unique II) instrument, for measuring the major elements. Detection limits for Si and Al are 100 and

120 ppm, respectively, and the values reported for other elements are Ca=55 ppm, Fe=15 ppm, K=20 ppm, Mg=30 ppm, Na=35 ppm, Mn=4 ppm and P=135 ppm. Trace-elements and REE were determined by ICP-MS using an ELAN DCR-E instrument at the department of the Geological Sciences, University of Colorado at Boulder. USGS standards were used as the calibration standards and to monitor accuracy during ICP-MS analysis (Saadat and Stern 2011). Precision for this analytical technique as determined by repeat analysis of the standards is generally better than 5% at the 95% confidence level (Saadat and Stern 2011). Methods for ICP-MS are similar to those described by Briggs (1996).

Isotopic analyses were done in the isotope lab in the Department of the Geological Sciences, University of Colorado. Isotopic measurements were carried out on powders of leached whole-rock material. Rock powders for isotopic analysis were generated in a ceramic-lined container. $^{87}Sr/^{86}Sr$ ratios were analyzed using Finnigan-Mat 261 four-collector static mass spectrometer. Replicate analyses of the SRM-987 standard in this mode yielded a mean $^{87}Sr/^{86}Sr$ of 0.71025±2 (2σ). Measured $^{87}Sr/^{86}Sr$ were corrected to SRM-987 = 0.710299±8. Errors are 2σ of the mean which refer to last two digits of the $^{87}Sr/^{86}Sr$ ratio. The Nd isotopic compositions are reported as ϵ_{Nd} values using a reference $^{143}Nd/^{144}Nd_{CHUR}$ ratio of 0.512638. Measured $^{143}Nd/^{144}Nd$ was normalized to $^{146}Nd/^{144}Nd$ = 0.7219. Analyses were dynamic mode, three-collector measurements. 33 measurements of the La Jolla Nd standard during the study period yielded a mean $^{143}Nd/^{144}Nd$ =0.511843 ±8 (2σ mean), and as a result static mode $^{143}Nd/^{144}Nd$ ratios determination for unknowns were corrected upwards to agree with the dynamic mode analyses. Pb isotopic analyses were four-collector static mode measurements. Sixteen measurements of SRM-981 during the study period yielded $^{208}Pb/^{204}Pb$= 36.56±0.03, $^{207}Pb/^{204}Pb$= 15.449±0.008, $^{206}Pb/^{204}Pb$ = 16.905 ±0.007 (2σ mean). Measured Pb isotope ratios were corrected to SRM-981 values ($^{208}Pb/^{204}Pb$= 36.721, $^{207}Pb/^{204}Pb$ = 15.491, $^{206}Pb/^{204}Pb$= 16.937). Total procedural blanks averaged ~1 ng for Pb and Sr, and 100 pg for Nd during study period. No age correction was applied to the data because of the young age of the rocks. Details of analytical procedures are given in Farmer et al. (1991, 2002).

4. Results

4.1. Petrography

Twenty-four samples were collected from the Paleogene volcanic rocks in the center of the Lut block and within the northern extension of the Sistan suture zone (Fig. 1). Basalts are dark colored, compact and occasionally contain vesicles. They have mainly porphyritic texture, containing 10% to 15% sub to euhedral olivine (0.5-1.5 mm and rarely up to 4mm in diameter) ± clinopyroxene (0.5-1.5 mm in diameter) and/or plagioclase (1-3 mm in diameter) phenocrysts. Groundmass textures are microcrystalline and vary between trachytic, intersertal and intergranular with subhedral olivine, lath-like plagioclase, and clinopyroxene as the dominant phases. Just in one sample (C31-2, micro gabbro), phlogopite is present. Ti-magnetite, ilmenite, magnetite and chromium spinel also are present as accessory minerals. In some samples plagioclase laths are embedded in subhedral and anhedral phenocrysts of augite clinopyroxene resulting in subophitic texture. Apatite is an accessory mineral. Small amounts of chlorite and secondary calcite occur in fractures and vesicles in some samples, which are otherwise fresh and unaltered.

Andesitic samples have porphyritic texture containing phenocrysts from 0.5 mm to 4 mm in size. Pyroxenes (both clinopyroxene and orthopyroxene) and plagioclase are common phenocrysts. The groundmass also consists mainly of plagioclase laths, pyroxene and accessory alkali feldspar. In addition, opaque minerals (magnetite, ilmenite) and apatite, are present in the groundmass. Minor amounts of secondary calcite, clay mineral, serecite and chlorite occur in some samples. More detail description of andesitic and dacitic rocks from the eastern and northern Lut block can be found in Jung et al. (1984) and Pang et al. (2013).

4.2. Mineral compositions

4.2.1. Olivine

The core compositions of the olivine phenocrysts from Lut block basalts range between Fo_{64} to Fo_{90} (Table 2). These have relatively Mg-rich cores (Fo_{84} to Fo_{90}) mantled by thinner less forsteritic rim (Fo_{64} to Fo_{80}, Table 2). The cores also have higher NiO contents than the rims. Microliths of olivine show similar compositions to the rim of the olivine phenocrysts.

4.2.2 Clinopyroxene

Clinopyroxene phenocrysts are very homogenous and show a very small range in composition from Wo_{42-46}, En_{42-48}, and Fs_{6-12} (Table 3). The amount of TiO_2 in clinopyroxenes from these samples range from 0.29 wt. % to 0.98 wt. %. Al_2O_3 in clinopyroxenes ranges from 1.7 to 4.6 wt. % and Cr_2O_5 ranges from 0.01 to 0.99 wt. % (Table 3).

Table 2. Representative electron microprobe analyses of olivine.

Sample	C8		C12		C31-2	C21	
	core	rim	core	rim	core	core	rim
No.	4	2	2	2	3	2	2
SiO_2	39.8	39.1	40.7	39.1	37.2	41.8	39.0
FeO	15.36	23.64	13.04	21.31	30.3	10.1	17.89
MnO	0.23	0.42	0.2	0.54	1.1	0.16	0.35
NiO	0.13	0.05	0.31	0.12	0.01	0.33	0.16
MgO	44.9	37.9	47.4	39.9	31.2	49.8	42.0
Total	100.3	101.1	101.5	101.0	99.8	102.2	99.4
Cation calculated based on 4 oxygen							
Fe	0.322	0.513	0.216	0.414	0.691	0.203	0.384
Mn	0.005	0.009	0.003	0.010	0.025	0.003	0.008
Ni	0.003	0.001	0.006	0.002	0.000	0.006	0.003
Mg	1.67	1.46	1.78	1.57	1.27	1.78	1.60
Fo	84	73	86	76	64	90	80

4.2.3. Feldspar

The compositional range of plagioclase (mainly in the groundmass) from central and eastern Lut block samples is An_{39-62}. Rare K-feldspar in the groundmass show compositions which vary from Or_{53} to Or_{71} (Table 4).

4.3. Whole rock compositions

4.3.1 Major elements

The major and trace element concentrations of the Paleogene basaltic samples (SiO_2 ~ 48-52 wt. %) from the north-central and eastern part of the Lut block are presented in Table 5. The major and trace element concentrations of andesitic samples (SiO_2 ~ 54-64 wt. %) from north-central and eastern Lut block is shown in Table 6. Samples analyzed in this study plot in the both alkaline and subalkaline fields (Fig.2). The chemical composition of the basaltic rocks mainly plot on the alkaline basalt or hawaiite field on silica versus total alkalis classification diagram(Fig. 2). Intermediate rock samples (SiO_2 ~54-61 wt. %) in this area include basaltic andesites, andesites, trachtandesites, and dacites (Fig. 2). Normative nepheline of the Paleogene basaltic samples from the north-central and eastern Lut block samples varies from absent to 10%, whereas the Neogene alkaline olivine basalts from the western part of the Lut block contain normative nepheline up to 16%. The highest value of normative nepheline from central and eastern Lut block samples refers to a sample of microgabbro (C31-2), which has phlogopite in its mineral assemblage. This mineral is unstable at the high temperatures of the convecting upper mantle and therefore implies basalt derivation from, or interaction with, the lithospheric mantle (Class and Goldstein 1997).

K_2O versus Na_2O diagram (Fig. 3) shows that some of these Paleogene samples from the north-central Lut black, unlike the young Neogene basaltic samples from the margins of the Lut block, mostly plot in the K-series field, although some plot in the Na-series field as well, but some of them belong to the K-series or high K-series. The MgO versus TiO_2 diagram indicates that the Paleogene samples generally plot on the low-Ti field, whereas the Quaternary and Neogene alkali basalts from the margins of the Lut block have higher Ti contents (Fig. 3). Just two Paleogene basaltic samples, D from the eastern part of the study area and BS-2 from north-east of the Nayband fault, show high Ti value similar to Neogene basalts collected from the margins of the Lut block (Fig. 3). Basaltic samples have moderate to high MgO (3.4–12.8 wt. %) and Al_2O_3 (11.5–16.8 wt. %; Table 5). Both basaltic and andesitic samples indicate positive correlation between CaO/Na_2O versus MgO, whereas SiO_2 contents show negative correlations with MgO which are interpreted to result from fractionation of clinopyroxene and/or olivine (Fig. 4).

Table 3. Representative electron microprobe analyses of clinopyroxene.

Sample	**C 12**					**C 21**			
CPX	**core**	**core**	**core**	**rim**	**core**	**core**	**core**	**core**	**rim**
SiO_2	51.44	51.71	51.16	49.09	50.45	49.58	50.3	52.88	48.13
TiO_2	0.47	0.44	0.52	0.98	0.37	0.96	0.57	0.29	0.75
Al_2O_3	2.41	1.85	2.34	3.22	3.46	3.98	3.02	1.71	4.59
Cr_2O_3	0.66	0.66	0.82	0.01	0.99	0.13	0.02	0.20	0.11
FeO	4.17	3.84	3.88	6.36	4.13	6.93	6.79	5.84	7.18
MnO	0.11	0.17	0.14	0.17	0.15	0.26	0.28	0.22	0.19
MgO	16.38	16.66	16.49	14.89	16.05	15.01	15.89	17.23	14.23
CaO	22.60	22.70	22.34	22.18	20.83	21.87	21.57	21.17	22.11
Na_2O	0.46	0.40	0.53	0.42	0.75	0.40	0.27	0.27	0.31
Total	98.71	98.44	98.22	97.33	97.18	99.13	98.71	99.82	97.61
Cations calculated on the basis of 6 oxygens									
Si	1.901	1.915	1.897	1.855	1.888	1.841	1.871	1.937	1.818
Al	0.105	0.081	0.102	0.144	0.153	0.174	0.133	0.074	0.204
Ti	0.013	0.012	0.015	0.028	0.01	0.027	0.016	0.008	0.021
Cr	0.019	0.02	0.024	0.000	0.029	0.004	0.001	0.006	0.003
Fe	0.129	0.119	0.120	0.201	0.129	0.215	0.211	0.179	0.227
Mn	0.004	0.005	0.004	0.005	0.005	0.008	0.009	0.007	0.006
Mg	0.902	0.92	0.912	0.839	0.895	0.831	0.881	0.94	0.801
Ca	0.895	0.901	0.888	0.898	0.835	0.870	0.860	0.830	0.895
Na	0.033	0.029	0.038	0.031	0.054	0.029	0.02	0.019	0.023
En	46.9	47.4	47.5	43.3	48.1	43.4	45.1	48.2	41.7
Wo	46.5	46.4	46.2	46.3	44.9	45.4	44	42.6	46.5
Fs	6.7	6.1	6.3	10.4	6.9	11.2	10.8	9.2	11.8
Mg#	89	90	90	83	89	82	83	86	81

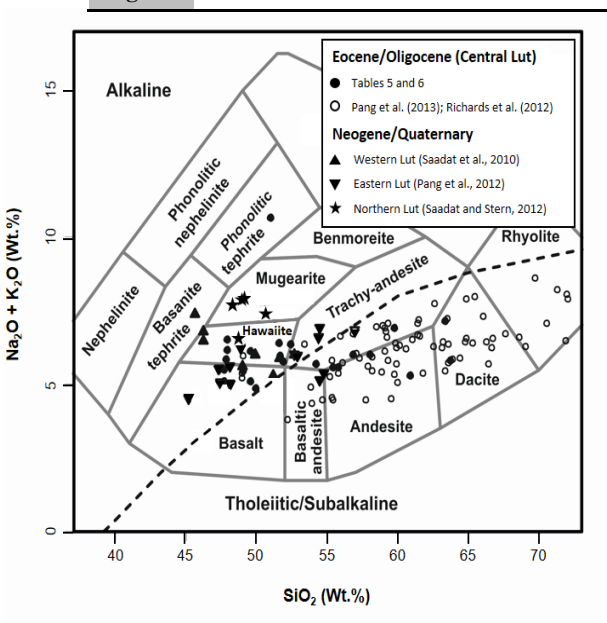

Fig. 2. Geochemical division of rocks based on Na_2O+K_2O (wt.%) versus SiO_2 (wt.%), modified from Cox et al. (1979). The heavy dashed dividing line between the subalkaline and alkaline fields is from Myashiro (1978).

Table 4. Representative electron microprobe analyses of plagioclase

Sample	C-21		C8		C12		D		C31-2	
No.	3	1	3	1	1	2	1	2	1	2
SiO_2	52.55	65.64	58.21	52.17	66.32	56.02	65.69	57.46	61.91	54.73
Al_2O_3	29.48	19.19	26.23	29.87	19.69	27.64	19.39	26.91	19.82	29.15
FeO	1.06	0.44	0.67	1.06	0.32	0.74	0.38	0.90	0.73	0.28
CaO	12.05	0.70	8.09	12.18	0.67	9.61	0.67	8.66	1.36	10.62
Na_2O	3.96	4.04	6.69	3.95	4.87	5.52	5.14	6.20	2.14	4.85
K_2O	0.34	10.81	0.47	0.19	9.82	0.32	9.44	0.44	10.8	0.44
Total	99.45	100.82	100.36	99.42	101.69	99.85	100.72	100.56	96.75	100.07
Number of ions basis of 32 oxygen										
Si	9.62	11.83	10.40	9.56	11.79	10.13	11.77	10.28	11.76	9.89
Al	6.36	4.08	5.52	6.45	4.13	5.89	4.10	5.67	4.44	6.21
Fe	0.16	0.07	0.10	0.16	0.05	0.11	0.06	0.13	0.12	0.04
Ca	2.36	0.13	1.55	2.39	0.13	1.86	0.13	1.66	0.28	2.06
Na	1.41	1.41	2.32	1.40	1.68	1.93	1.79	2.15	0.79	1.70
K	0.08	2.48	0.11	0.04	2.23	0.07	2.16	0.10	2.62	0.10
Or	2	62	3	1	55	2	53	3	71	3
Ab	37	35	58	37	42	50	44	55	21	44
An	61	3	39	62	3	48	3	42	8	53

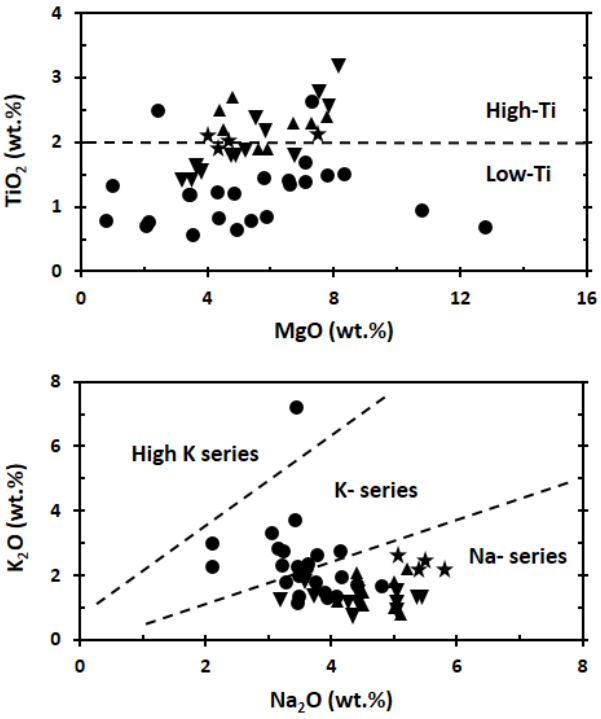

Fig. 3. TiO_2 versus MgO and K_2O versus Na_2O diagram after Middlemost (1975). The symbols are the same as shown in Figure 2.

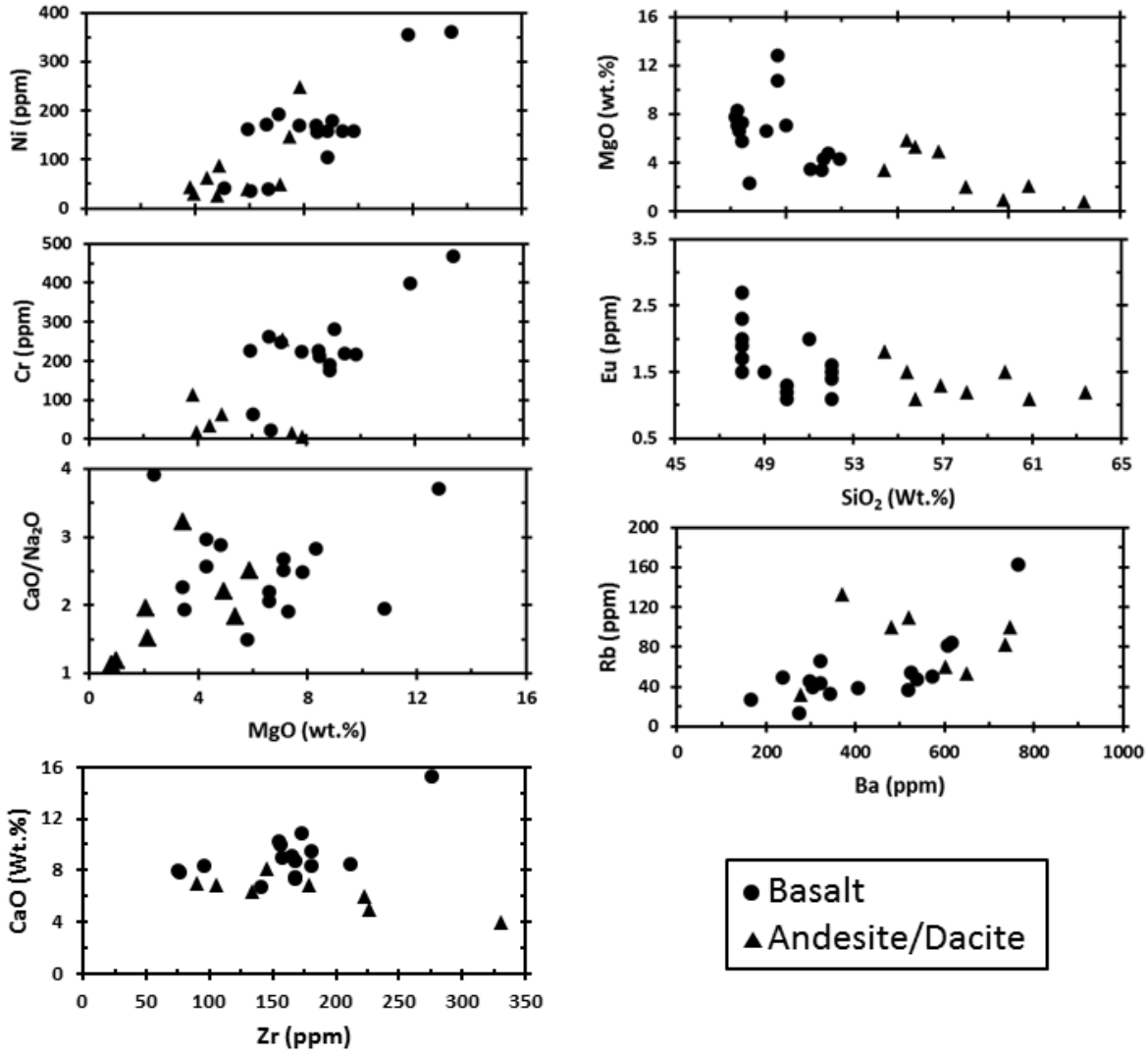

Fig. 4. Plots of MgO versus CaO/Na_2O, Ni and Cr, SiO_2 versus Eu and MgO, CaO against Zr, and Ba versus Rb.

4.3.2 Compatible and Incompatible Trace Elements

Trace elements concentrations of Paleogene basaltic samples from north-central and eastern Lut block are presented in Table 5 and for andesitic samples in Table 6. The concentrations of Ni vary from 36 to 361 ppm for the basalts, and chromium in these samples varies between 8 to 469 ppm. In comparison, the Neogene alkali olivine basalts from western Lut block contain lower concentrations of Ni (123 ppm on average; Saadat et al. 2010). Chromium and nickel both indicate positive correlation with MgO (Fig. 4).

Nickel is a sensitive indicator of olivine fractionation/ accumulation from basaltic magmas because of its large partition coefficient (mineral/melt concentration), and the data suggest that the decreasing MgO and Ni is due, in part, to olivine fractionation, while decreasing Cr may result from clinopyroxene fractionation (Fig. 4). There is a negative correlation between Eu and SiO_2 and positive correlation between Rb and Ba and also between CaO and Zr in basaltic samples (Fig. 4). A weak negative Eu anomaly in normalized REE andesite/dacite samples (Fig. 5) and also decreasing concentrations of CaO versus Zr (Fig. 4) indicate plagioclase fractionation is dominant in andesite/ dacite samples.

Chondrite-normalized values of trace-element abundances for north-central and eastern Lut Paleogene basaltic and andesitic samples are presented in Figure 5. These samples are enriched in LREE relative to HREE and the values of $(La/Yb)_N$ vary from 5.3 to 18.1 (Table 5). These values vary from 6 to 21 for Neogene basalts from the western part of the Lut block (Saadat et al. 2010). Depletions in Nb relatively to

LILE (Ba, Sr) and other characteristics, such as low TiO_2 and high Ba/La and Ba/Nb ratios (Table 5, Fig. 5) for the basalts and andesitic samples from the north-central and eastern Lut block (Fig. 5), suggest affinities, at least for some of these samples, with convergent plate boundary arc magmas. In contrast, the low La/Nb and Ba/Nb ratios and normalized trace element patterns for Quaternary and Neogene alkali basalts from the western Lut are similar to oceanic island basalts (OIB; Saadat et al. 2010).

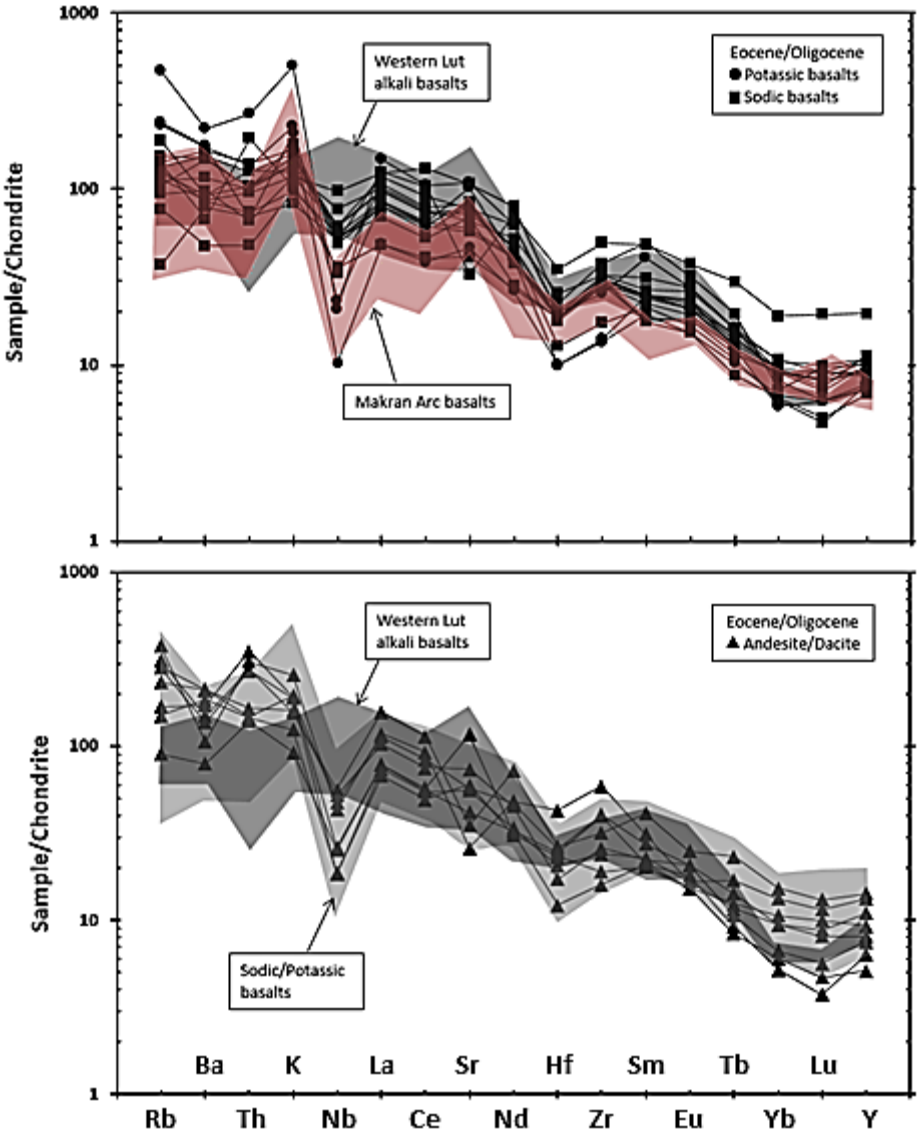

Fig. 5. Chondrite normalized multi-element spider diagram for potassic and sodic basalts and andesites and dacites from the north-central Lut block. Normalization values from Gerlach et al. (1988).

Table 5. Major element (in wt. % by XRF) and trace element (in ppm by ICP-MS) composition of basaltic samples from the north-central Lut block.

Sample	C31-2	C31-1	C23-2	C23-1	C22-5	C21	C12	C8	C7	C6	C5	C4	C3	C2	D	BS-2
SiO_2	51.0	52.0	52.0	52.0	52.0	50.0	50.0	50.0	49.0	48.0	48.0	48.0	48.0	48.0	48.0	48.0
TiO_2	0.6	0.8	1.2	1.2	1.2	0.7	1.0	1.4	1.4	1.5	1.5	1.4	1.5	1.7	2.7	2.5
Al_2O_3	17.0	17.0	16.0	16.0	17.0	12.0	14.0	16.0	16.0	15.0	15.0	16.0	16.0	16.0	15.0	16.0
FeO(total)	6.9	7.9	7.1	7.8	7.8	9.3	9.3	9.4	9.5	9.9	9.8	9.3	9.7	9.7	10.1	8.6
MnO	0.2	0.2	0.2	0.2	0.2	0.2	0.2	0.2	0.2	0.2	0.2	0.2	0.2	0.2	0.1	0.2
MgO	3.5	4.3	4.3	4.8	3.4	12.8	10.8	7.1	6.6	8.3	7.8	6.6	5.8	7.1	7.3	2.4
CaO	6.6	7.7	10.7	10.1	8.6	7.8	8.2	8.8	9	9.9	8.2	7.4	7.2	9.4	8.4	15.2
Na_2O	3.4	3.0	3.6	3.5	3.8	2.1	4.2	3.5	4.1	3.5	3.3	3.6	4.8	3.5	4.4	3.9
K_2O	7.2	3.3	2.4	2.3	2.6	3.0	2.0	1.4	1.4	1.2	1.8	2.2	1.7	2.0	1.7	1.5
P_2O_5	0.8	0.3	0.3	0.3	0.3	0.3	0.3	0.3	0.5	0.5	0.5	0.5	0.5	0.6	0.6	0.6
Total	97.2	96.5	97.8	98.2	96.9	98.2	100	98.1	97.7	98.0	96.1	95.2	95.4	98.2	98.3	98.9

Sample	C31-2	C31-1	C23-2	C23-1	C22-5	C21	C12	C8	C7	C6	C5	C4	C3	C2	D	BS-2
Ni	36	39	171	193	162	361	355	105	170	159	158	156	170	158	178	41.7
Cr	63	22	261	247	226	469	399	190	227	216	219	211	224	177	281	8.4
V	236	289	174	165	158	225	203	194	208	218	200	187	207	214	312	178.4
Cs	6.6	0.9	1.2	0.9	0.7	2.7	0.7	1.7	0.8	0.6	0.8	1.2	0.7	0.3	1.3	1
Rb	163	81	50	47	54	84	37	27	45	13	43	66	40	39	33	48.9
Ba	766	607	572	538	524	615	519	166	297	275	322	322	304	405	343	236.8
Sr	1200	1118	924	898	761	508	902	452	653	629	725	802	831	850	1175	361.6
Nb	8	9	20	19	21	4	13	14	22	20	30	24	24	24	38	19.5
Ta	2.5	0.6	2.1	2	1.5	0.4	1.4	1	1.7	1.3	4.9	1.2	1.3	1.5	5.4	1.4
Zr	142	78	174	156	169	76	97	159	166	157	182	169	169	182	213	276.6
Y	17	16	20	19	15	16	17	20	21	24	24	22	23	25	22	43.1
Hf	3.6	1.8	3.7	3.4	3.3	1.8	2.3	3.3	3.4	3.2	4.6	3.3	3.3	3.5	4.0	6.3
Th	13.3	6.8	7.0	6.3	5.1	3.4	5.2	2.4	3.7	3.5	6.4	5.2	4.8	5.0	3.3	9.7
U	7.3	4.0	4.1	3.4	3.5	2.3	0.8	1.3	1.8	1.6	2.1	1.9	1.8	1.9	0.7	2.0
Pb	17.4	9.3	5.0	4.2	9.1	7.5	6.0	3.8	4.0	4.6	4.2	4.1	4.6	2.6	4.9	16.8
La	46.5	27.0	26.5	25.1	21.8	15.3	33.8	15.2	26.8	25.3	31.9	31.0	30.7	36.9	39.0	39.2
Ce	84.8	52.6	51.0	47.2	42.7	31.2	63.6	33.1	52.8	50.1	61.5	58.5	59.6	73.5	106.0	84.0
Pr	9.3	5.7	5.6	5.4	4.3	3.7	6.9	3.7	5.7	5.9	6.7	6.2	6.5	8.5	13.0	9.9
Nd	37.5	23.9	23.1	22.4	17.0	15.8	27.4	16.3	24.5	24.2	31.2	28.0	27.6	37.4	48.0	42.5
Sm	7.8	4.7	4.8	4.3	3.4	3.7	4.1	3.5	4.6	4.8	5.1	4.8	4.7	6.0	9.4	9.3
Eu	2.0	1.5	1.6	1.4	1.1	1.1	1.2	1.3	1.5	1.5	1.9	1.7	1.7	2.0	2.3	2.7
Gd	8.3	5.0	5.3	4.6	3.7	3.5	5.2	4.4	5.5	5.4	5.8	5.2	5.8	6.7	7.7	11.3
Tb	0.8	0.6	0.7	0.6	0.4	0.5	0.5	0.6	0.6	0.8	0.8	0.6	0.7	0.8	1.0	1.5
Yb	1.7	1.2	2.0	1.9	1.4	1.4	1.3	1.9	2.0	2.2	2.2	1.9	1.9	2.0	1.5	4.0
Lu	0.2	0.2	0.3	0.3	0.2	0.2	0.2	0.3	0.3	0.3	0.3	0.2	0.3	0.2	0.3	0.6
Ba/Nb	91.2	71.4	28.3	28.9	24.4	143.5	41.0	12.0	13.4	13.5	10.6	13.2	12.7	17.1	9.0	12.1
La/Nb	5.5	3.2	1.3	1.3	1.0	3.6	2.7	1.1	1.2	1.2	1.0	1.3	1.3	1.6	1.0	2.0
Sr/Nb	150.0	124.2	46.2	47.3	36.2	127.0	69.4	32.3	29.7	31.5	24.2	33.4	34.6	35.4	30.9	18.6
$(La/Yb)_N$	18.1	15.1	8.9	8.9	10.6	7.4	17.1	5.3	9.1	7.5	9.6	10.8	10.7	12.4	17.2	6.6

Table 6. Major element (in wt. % by XRF) and trace element (in ppm by ICP-MS) composition of andesites/dacites samples from the north-central Lut block

Sample	C30-1	C28	C25	C20-1	C13	C11	C10	BS-1
SiO_2	56.9	55.8	58.1	55.4	59.8	63.4	60.9	54.4
TiO_2	0.7	0.8	0.7	0.9	1.3	0.8	0.8	1.2
Al_2O_3	15.5	16.0	16.8	14.2	16.8	16.2	16.3	19.2
TFeO	6.9	7.2	6.9	7.3	6.1	4.8	5.8	9.8
MnO	0.2	0.2	0.2	0.2	0.2	0.1	0.2	0.1
MgO	4.9	5.4	2.1	5.8	1.0	0.8	2.1	3.4
CaO	7.0	6.9	6.3	8.1	5.0	3.9	6.0	6.8
Na_2O	3.2	3.7	3.2	3.2	4.1	3.4	3.9	2.1
K_2O	2.8	1.8	2.8	2.3	2.8	3.7	1.3	2.3
P_2O_5	0.3	0.2	0.2	0.3	0.3	0.2	0.2	0.2
Total	98.2	97.9	97.3	97.6	97.3	97.3	97.5	99.5

4.4. Radiogenic isotopes

Sr–Nd–Pb isotopic ratios for the basalts and andesitic basalts from the central and eastern Lut block are given in Table 7. The $^{87}Sr/^{86}Sr$ ratios for selected samples from the center and eastern Lut block range from 0.703827 to 0.705063 and $^{143}Nd/^{144}Nd$ ratios range from 0.512681 to 0.512871 (Table 7, Fig. 6). These values overlap previously published isotopic ratios for Paleogene igneous rocks from the central Lut block (Fig. 6; Pang et al. 2013), and are higher than Bulk Earth $^{87}Sr/^{86}Sr$ and $^{143}Nd/^{144}Nd$ ratios. They are also similar to the $^{87}Sr/^{86}Sr$ and $^{143}Nd/^{144}Nd$ ratios for Neogene/Quaternary alkali basalts from the western, eastern and northern Lut block (Saadat et al. 2010; Saadat and Stern 2012; Pang et al. 2012), as well as to Quaternary Makran arc basalts to the south (Saadat and Stern 2011). There are no available isotopic data values for local basement.

The Pb isotopic composition of basalts and andesitic basalts from the central and eastern Lut block plot above the Northern Hemispheric Reference Line (NHRL), and range from 38.449 to 38.870, 15.553 to 15.680 and 18.500 to 18.798 for $^{208}/^{204}Pb$, $^{207}/^{204}Pb$, respectively (Table 7, Fig. 7).

Table 7. Sr, Nd, and Pb isotopic composition of andesite and basalts samples from the north-central Lut block.

4. Discussion

5.1. Temporal distribution of volcanism

Within the north-central, eastern, and western Lut block the surface areas covered by volcanic rocks have varied with time (Fig. 8). The data were grouped according to the ages reported in geological maps, which are mainly inferred from stratigraphic relationships. Ages obtained from isotopic methods are also considered. The results that are displayed in this diagram, which plots area of erupted material versus time, indicate that between 65 to 56 Ma (Paleocene), the north-central, eastern, and western Lut block was covered by just around 730 km^2 of volcanic rocks. In contrast, from 56 to 34 Ma (Eocene), the total areas of volcanic provinces covered an area more than 16,000 km^2 (Fig. 8). The eruption rate decreased markedly during Oligocene and Neogene/Quaternary times to ~3.800 km^2 and ~3,300 km^2, respectively.

Although the older volcanic centers might be more eroded or covered by recent deposits and there is no estimation of the thickness of lavas or pyroclastic flows in this area, nor the volume of subvolcanic plutons. Nevertheless, based on the surface area covered by volcanic rocks, the overall rate of magmatism ranged from 75 km^2/m.y. to 745 km^2/m.y. from Paleocene to Eocene. This number ranged from 350 km^2/m.y. to 145 km^2/m.y. for Oligocene and Neogene/Quaternary, respectively. This suggests that the maximum volcanic activities took place during Eocene time, and then it dramatically decreased to present.

The present level of data is not sufficient to recognize distinct temporal and spatial patterns emerging from the Paleogene magmatic activity in the north-central Lut block volcanism.

However, for the alkali olivine basalts erupted along the western and eastern margins of the Lut block during the Neogene/Quaternary, there is a clear pattern of the migration of this volcanism with time from north to south.

Table 6. Continued

Sample	C30-1	C28	C25	C20-1	C13	C11	C10	BS-1
Ni	48	146	26	249	30	43	86	40
Cr	83	255	15	286	5	19	114	35
V	227	169	209	166	136	74	120	181
Cs	1	3	70	3	6	12	1	2
Rb	82	53	60	100	100	133	32	109
Ba	737	651	603	747	482	372	278	521
Sr	1294	663	614	813	633	286	461	387
Nb	10.2	7.3	7.2	20.5	18.6	16.9	9.9	22.0
Ta	1.2	4.4	1.2	1.5	1.6	3.9	1.9	1.8
Zr	90.2	106.6	134.2	146.3	227.4	331.6	223.0	178.8
Y	14.0	11.3	17.9	16.6	24.2	29.4	20.5	31.4
Hf	2.2	4.2	3.7	3.1	4.6	7.7	4.4	4.8
Th	7.4	7.3	17.6	8.3	13.6	15.4	7.0	13.9
U	4.4	3.2	11.0	3.5	5.6	2.6	3.1	2.7
Pb	13.2	15.7	16.5	9.1	15.1	17.9	7.6	11.6
La	24.7	21.3	23.4	32.5	35.7	37.3	24.7	49.6
Ce	46.9	40.2	44.8	61.2	68.8	75.6	45.4	92.9
Pr	5.00	4.50	5.10	6.30	7.20	7.70	4.90	10.00
Nd	19.3	18.5	20.2	27.1	28.5	28.8	19.5	43.2
Sm	4.00	3.90	4.40	4.30	5.30	6.00	4.10	7.90
Eu	1.30	1.10	1.20	1.50	1.50	1.20	1.10	1.80
Gd	4.20	4.10	5.10	4.70	6.20	7.00	4.90	9.70
Tb	0.45	0.41	0.57	0.52	0.70	0.83	0.61	1.14
Yb	1.08	1.25	1.96	1.39	1.96	2.77	2.21	3.18
Lu	0.12	0.15	0.26	0.18	0.28	0.37	0.32	0.42
Ba/Nb	72.10	89.40	83.60	36.40	25.90	22.00	28.10	23.70
La/Nb	2.40	2.90	3.20	1.60	1.90	2.20	2.50	2.30
Sr/Nb	126.50	91.10	85.10	39.60	34.00	17.00	46.50	17.60
$(La/Yb)_N$	15.10	11.30	7.90	15.50	12.00	8.90	7.40	10.30

Table 7. Sr, Nd, and Pb isotopic composition of andesite and basalts samples from the north-central Lut block.

Sample No.	Rock type	$^{87/86}Sr$	$^{143/144}Nd$	ƐNd	$^{208/204}Pb$	$^{207/204}Pb$	$^{206/204}Pb$
D	Hawaiite	0.705063±0.00006	0.512732±0.00012	1.83	38.702	15.558	18.629
C-8	Basalt	0.703827±0.00013	0.512871±0.00017	4.54	38.449	15.553	18.500
C-12	Hawaiite	0.704647±0.00013	0.512765±0.00014	2.48	38.837	15.560	18.798
C-21	Basalt	0.705056±0.00013	0.512692±0.00015	1.05	38.870	15.568	18.790
C-28	Andesite	0.704891±0.00013	0.512681±0.00013	0.84	38.714	15.560	18.674

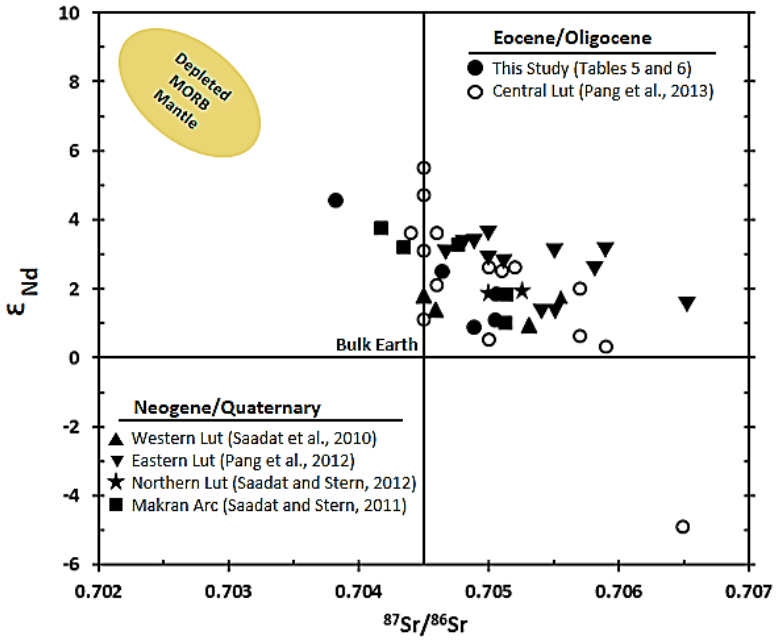

Fig. 6. $^{87}Sr/^{86}Sr$ ratio versus ε_{Nd} comparing north-central Lut block samples with other alkali basalts around the Lut block and northeastern Iran.

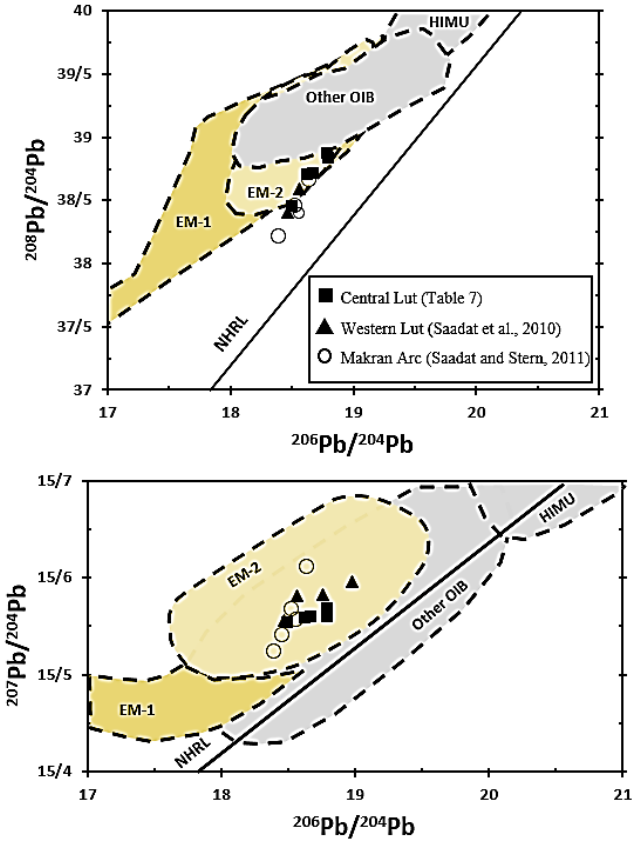

Fig. 7. Plot of $^{207}Pb/^{204}Pb$ and $^{208}Pb/^{204}Pb$ versus $^{206}Pb/^{204}Pb$. Base diagram from Hofmann (1997). NHRL= Northern Hemisphere Reference Line (Hart, 1984).

Geochronological data for alkaline basalts erupted along the northern part of Nehbandan Fault, the western margin of the Lut block (Fig. 1), yield ages of about 14-15 Ma for the northernmost outcrops (Jung et al. 1984; Pang et al. 2012), and of 2.2-2.6 Ma (Conrad et al. 1981; Walker et al. 2009; Chiu at al. 2013) for samples from further south, along the middle of the Nayband fault, also called Gandom Beryan (Saadat et al. 2010). Along the eastern margin of the Lut block, the alkali basalts yield ages between 10-11 Ma at northern end of the Nehbandan fault (Fig. 1), whereas further to the south, along the southern part of the Nehbandan fault, alkali basalts erupted at 1.5-1.7 Ma (Conrad et al. 1981; Pang et al. 2012; Chiu et al. 2013), thus showing the same pattern of north to south migration as along the western margin of the Lut block.

5.2. Crustal Contamination

Based on both K/P and Ti/Yb versus $^{87}Sr/^{86}Sr$, and also Ce versus Ce/Pb, at least some of the central and eastern Lut block basaltic samples may have been affected by varying extents of crustal assimilation during ascent to the surface (Fig. 9). As pointed by Thompson et al. (1983), the K/P ratio is a good indicator of contamination, since K is enriched and P is depleted in typical upper crust. This ratio is higher for some potassic series basalts (e.g., 8.2 for C31-2, 11.7 for C31-1, and 10.1 for C21; Table 5), but lower for sodic basalts (ranging from 2.7 to 8.2).

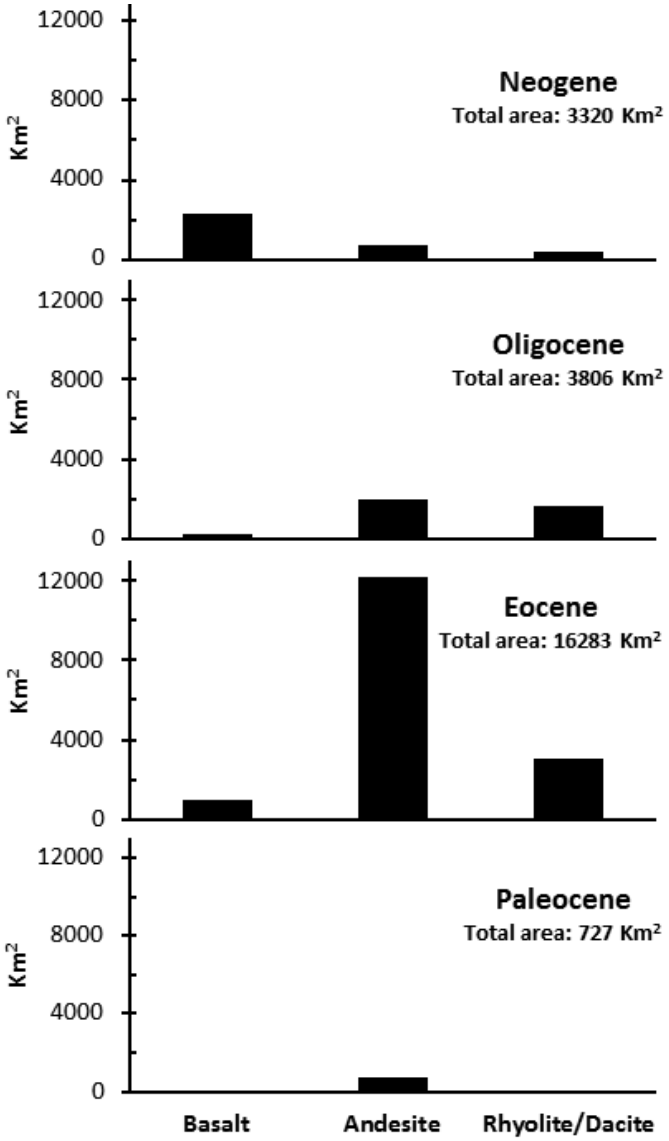

Fig. 8. Variations in intensity of magmatism in the north-central Lut block are plotted as surface areas covered by volcanic rocks of different compositions as function of time.

The lack of a positive relation in a plot of K/P ratio against $^{87}Sr/^{86}Sr$ ratio suggests that the higher than mantle K/P of some of the sample could be related to assimilation of lower, but not upper crust (Fig. 9). The role of upper crustal contamination can also be tested by at Ti/Yb ratios in conjunction with radiogenic isotope ratios (Leeman and Hawkesworth 1986; Van Calsterern et al. 1986; Carlson and Hart 1987). As pointed out by Leeman and Hawkesworth (1986), high Ti/Yb ratio strongly suggests that contribution from upper crustal material were minimal, but low Ti/Yb does not necessarily prove that crustal contamination took place. The low K/P (<3) and high Ti/Yb (>10000) of sample D from the eastern part of the Lut block (Fig. 9) indicates minimal or no upper crustal but possibly lower crustal contamination. Samples from middle part of the Lut block display higher values of K/P and lower values of Ti/Yb, also consistent with variable degree of interaction with lower crust (Fig. 9). In addition, although Ce/Pb ratio of all the samples varies between 2.5 and 28 (Fig. 9), the lowest values are for the K-series basalts and andesites, indicating that some of them may have been affected by low degrees of lower crustal contamination. However, most of the Na-series basalts, which have Ce/Pb >10 (Fig. 9), are derived from mantle sources unaffected by crustal contamination (Hofmann et al. 1986; Sims and DePaolo 1997)

5.3. Fractional Crystallization

The strong positive correlation between CaO/Na_2O versus MgO, whereas SiO_2 contents show negative correlations with MgO (Fig. 4). These trends are interpreted as fractionation of clinopyroxene and olivine from parental basaltic magmas. The compatible trace elements Ni and Cr support this observation that these samples all experienced some crystal fractionation. Relatively strong positive correlation of nickel with MgO is interpreted as the presence of olivine in the fractionating assemblage (Fig. 4). The positive correlation of chromium with MgO could be related to crystallization of clinopyroxene and/or a Cr-rich spinel phase.

Negative correlation between Eu and SiO_2 and positive correlation between Rb and Ba perhaps suggest that fractional crystallization also involved plagioclase (Fig. 4). The absence of negative Eu anomalies in normalized REE pattern, and also the positive correlation between CaO and Zr in basaltic samples (Fig. 4), suggests that plagioclase fractionation was not significant in basaltic samples. However, a weak negative Eu anomaly is present in andesite and dacite samples (Fig. 5), and also decreasing concentrations of CaO versus Zr, indicate that some degree of plagioclase fractionation occurred in andesite and dacite samples (Fig. 4).

5.4. Partial Melting

Trace-element compositions of alkali basalts from the north-central Lut block indicate that their parental magma were produced by generally low, but variable degrees of partial melting. $(La/Yb)_N$ values for basaltic samples of central Lut block varies from 5.3 to 18.1 (Table 5), and between 6.1 and 20.8 for samples from the western Lut block (Saadat et al. 2010). The $(La/Yb)_N$ ratio in lavas significantly increases from north to south along the western and eastern margin of the Lut block, indicate decreasing mantle partial melting to the south where the lavas are younger. However, it is hard to find any spatial or temporal trend in samples from the central Lut block.

A plot of LREE/HREE versus HREE, e.g. La/Yb versus Yb, is useful to assess degree of mantle partial melting and distinguish between melting in the spinel and garnet fields (Thirwall et al. 1994; Baker et al. 1997). There is a very small change in La/Yb ratio in spinel-facies melts compared with their mantle source (Fig. 10). In contrast, there are large changes in Yb in melts formed in garnet-facies mantle (Baker et al. 1997). Based on the La/Yb versus Yb of alkali basalts from the central and western Lut block and the melt modeling presented in Figure 10, neither a variables degree of partial melting of a spinel lherzolite nor a variables degree of partial melting of garnet lherzolite solely can generate the observed variation in La/Yb ratio with changing Yb. One explanation of the La/Yb versus Yb compositions of these alkali basalts involves mixing of small melt fraction from garnet-facies mantle with relatively larger melt fractions from spinel-facies mantle (Fig. 10). This model is similar to that proposed by Baker et al. (1997) in which the Quaternary intraplate volcanic rocks from Sana'a, western Yemen, result from mixing of melts from both spinel and garnet lherzolite facies.

5.5. Mantle source chemistry

There is significant variation in lava chemistry between Paleogene samples from the north-central Lut block compared to the Neogene and Quaternary alkali basalt samples from western and eastern margins of the Lut block. Volcanic units of the north-central Lut block follow both calc-alkaline and alkaline trend on alkali versus SiO_2 diagram (Fig. 2) and on the K_2O versus Na_2O diagram plot in the Na-Series, K-series, and high K-series fields (Fig. 3).

MgO versus TiO_2 diagram indicates that samples from the north-central Lut block generally plot on the low-Ti field. In contrast the Quaternary and Neogene basalts from the western (Saadat et al. 2010) and eastern (Pang et al. 2012) Lut block have higher Ti content (Fig. 3).

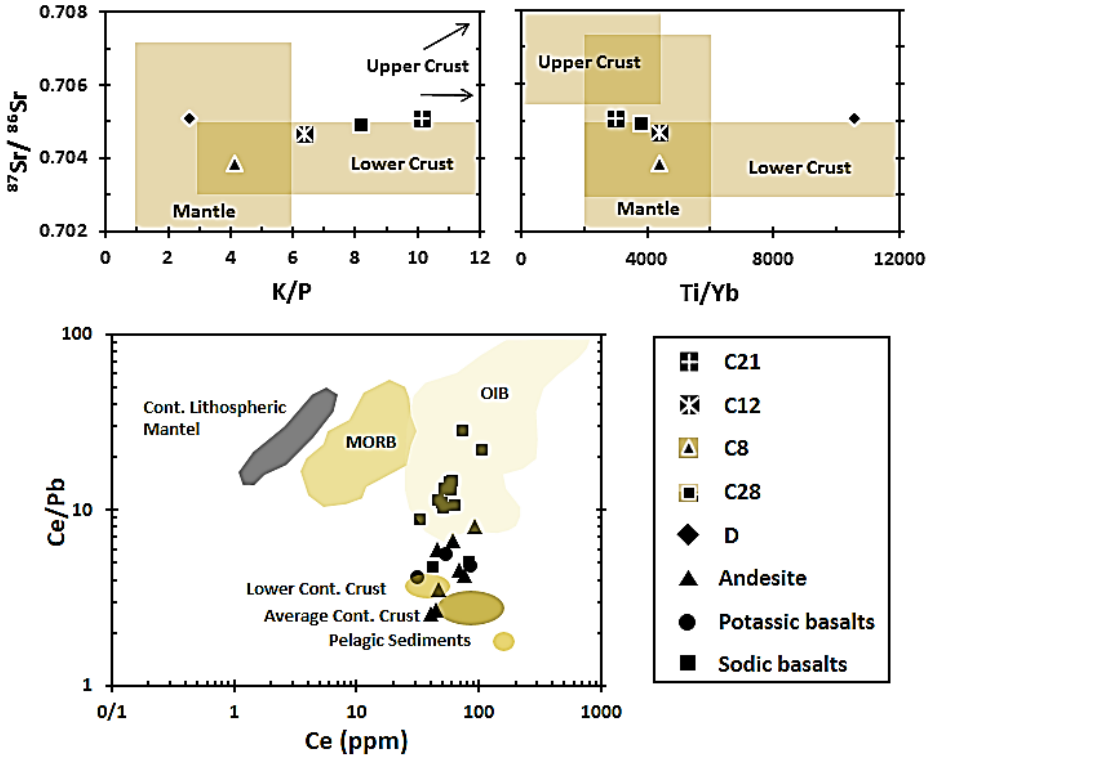

Fig. 9. Relationships between Sr isotopic composition and the ratios of K/P and Ti/Yb which are sensitive to crustal contamination (see text for discussion). Fields for mantle, upper and lower crust from Hart et al. (1988) and references therein. Ce/Pb versus concentration of Ce. Lower and total average continental crust is taken from Sims and DePaolo (1997) based on the average of four models of Rudnick and Fountain (1995), Taylor and McLennan (1985), Weaver and Tarney (1984) and Wedepohl (1994). An estimate for the continental lithospheric mantle is taken from Sims and DePaolo (1997) after McDonough (1990).

These Neogene samples also belong exclusively to the Na-series and display intra-plate alkaline characteristics derived from relatively primitive mantle, being very similar in trace element abundance patterns to the average composition of oceanic island basalt (OIB; Saadat et al. 2010; Pang et al. 2013). For the Paleogene volcanic rocks from the north-central Lut block, depletions in Nb relative to LILE (Ba, Sr, La), and other characteristics, such as low TiO_2 and high Ba/Nb and La/Nb ratios (Tables 5 and 6, Fig. 5) for both Na-series and K-series basalts and andesites, suggest affinities, at least for most of these samples, with convergent plate boundary arc magmas around the world. Calc-alkaline volcanic units from the north-central Lut block display chondrite-normalized trace-element patterns similar to the Makran continental arc volcanic rocks erupted along the southern margin of the Lut block (Fig. 5). This suggests that they possibly have been derived from an enriched mantle source containing a distinct subduction signature**.** This mantle source may have been in part the asthenosphere and in part in the lithosphere, as implied by the discussion in the previous section that suggests that melting of both these reservoirs participated in the generation of the north-central Lut block basalts.

Large-ion-lithophile element/high field strength element (LILE/HFSE) ratios, such as Sr/Nb, ratio has been found to be useful in showing the addition and variation of subduction related components (Farmer and Fornash 2009). In general, samples that are located in the northwest part of the central Lut block have significantly lower values (16-70) of this ratio than those located in the southwest part of the block (85-150; Fig. 11). The same trend occurs for Ba/Nb and La/Nb as well. We interpret these LILE/HFSE variations as an indication that subduction signature decreases to the north-northeast of the central Lut block. These ratios for Neogene alkaline olivine basalt which erupted along the western margin of the Lut block are low, similar to intra-plate OIB, and relatively constant (Saadat et al. 2010).

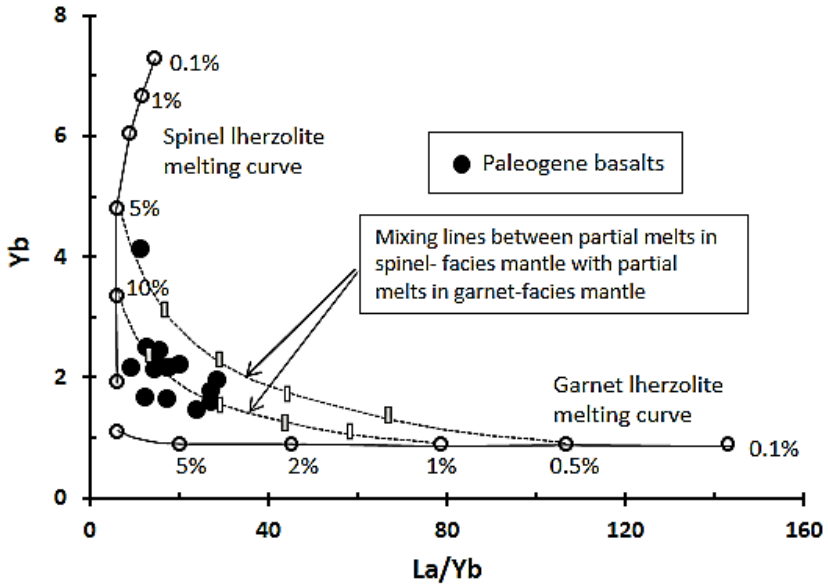

Fig. 10. Variation La/Yb versus Yb for the north-central Lut block samples. Factional melting curves for spinel and garnet lherzolite are taken from Baker et al. (1997) and references therein. The symbols are the same as in Fig. 2

5.6 Petrogenesis

The problem of how the large volume of Paleogene magmas, which have subduction-related geochemical signatures, were generated beneath the north-central Lut block in eastern Iran has been addressed in a number of previous studies (Jung et al. 1984; Ghorbani 1997; Vosughi Abedini 1997; Richards et al. 2012; Pang et al. 2013). One aspect of the problem is what oceanic crust was being subducted and in what direction. The ophiolitic rocks located on the northern margin of the Lut block probably resulted from closure of a branch of the Neotethys along a steeply northward dipping subduction zone (Spies et al. 1983, Shabanian 2012) and therefore are not related to the volcanism within the Lut block. Another possible source of subduction components comes from the eastern margin of the Lut block, where large ophiolite and melange bodies are remnants of the Cretaceous Sistan Ocean (Camp and Griffis 1982; Tirrul et al. 1983; Delavari et al. 2009).

This narrow ocean, which separated the Lut from the Afghan block, closed by middle Eocene (Camp and Griffis 1982), or during the Late Paleocene–Eocene (Bagheri and Stampfli 2008). Dercourt et al. (1986), Karimpour et al. (2005), Kazmin et al. (1986, 2010) and Pang et al. (3013) all conclude that Paleogene volcanism within the Lut block most likely was a result of the westward subduction of the Sistan Ocean. However, the polarity of the fore arc basin accretionary prism, the structural vergence in this prism, and the position of relatively high P/T metamorphic rocks on the inner eastern side of the prism, all suggest a northeast-dipping subduction system (Tirrul et al. 1983; Berberian et al. 1999; Fotoohi Rad 2005), although recently Arjmandzadeh et al. (2011) suggested two-sided asymmetric subduction of the Sistan Ocean beneath both Afghan to the east and the Lut blocks to the west, with different rates of consumption of oceanic lithosphere.

The geochemical data presented in this study does not show a pattern consistent with the origin of the Paleogene calk-alkaline volcanic rocks within the central Lut block resulting from the subduction of oceanic crust from the east. In contrast, LILE/HFSE ratios, interpreted as an indication of subduction signature, increase to the south-southwest of the central Lut block (Fig. 11), where Neotethyan oceanic crust was subducted beneath Iran along a northeast dipping subduction zone from approximately Late Triassic (Berberian and Berberian 1981) to Late Oligocene time (Fakhari et al. 2008). Verdel (2009) also suggested the mantle source of the Eocene-Oligocene volcanism in the north-central Lut block was metasomatized by slab-derived fluids over the course of ~150 million year, from the time of subduction initiation in the late Triassic until the late Eocene-early Oligocene.

Convergence rates of around 3 cm/yr during this period (Savostin et al. 1986), would have limited the volume of fluids released to the mantle wedge over any given period of time, but this supply of fluids was still sufficient to partially hydrate and alter the trace element composition of the mantle wedge, including both the subcontinental lithosphere and asthenosphere (Verdel 2009).

To account for the presence of subduction components derived from this subducting slab magmatism some 800 km inboard of the convergent plate margin active along the southwest margin of central and eastern Iran during the Paleogene time, low angle sub-horizontally subduction is required (Fig. 12a).

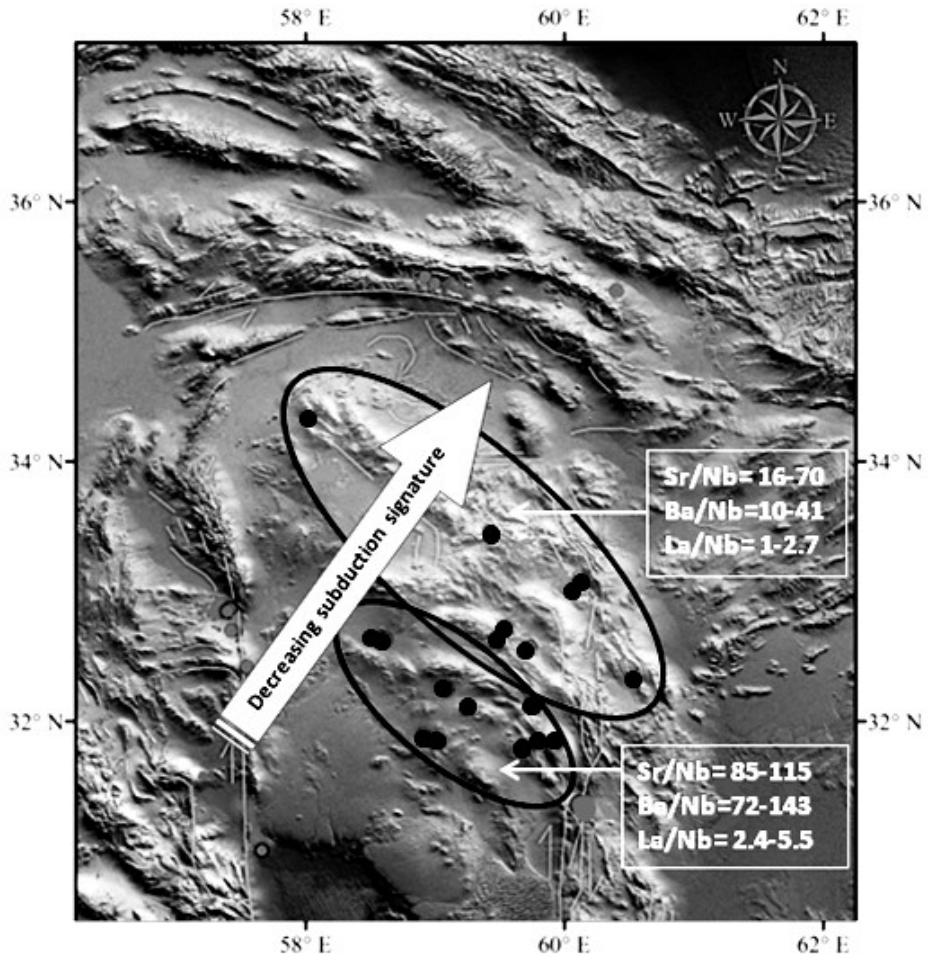

Fig. 11. Spatial variation of Sr/Nb, Ba/Nb and La/Nb ratios of Paleogene volcanic rocks within the north-central Lut block

During Late Eocene-Oligocene, the time of collision of the Arabian shield with Iran, the Lut block underwent uplift and no Oligocene-Miocene sediments were deposited (Bereberian 1974; Berberian and Soheili 1973). Since the beginning of the time this collision occurred, the rates of convergence between the two plates was slowed by ~35%, presumably because the thick continental crust of the Arabian shield made the subducting plate more buoyant than when only oceanic lithosphere was consumed (Hatzfeld and Molnar 2010). A decrease in the rate of Arabia-Eurasia convergence allowed the shallow slab to return to normal angle of subduction, accompanied by passive upwelling of hot temperature asthenospheric mantle into direct contact with portions of the subcontinental mantle lithosphere that had been previously hydrated and metasomatized by components derived from the lithosphere subducted between the Late Triassic and Late Eocene (Fig. 12b). Asthenospheric upwelling provided the heat to generate the voluminous mid to late Paleogene magmatism in this area (Ballmer et al. 2009). Support for this model comes from the mantle melting models (Fig. 10) that suggest that north-central Lut block Paleogene Na-series basalts are mixtures of both asthenospheric and lithospheric melts. The potassic basaltic samples within the Lut block are likely to have been derive from only metasomatized subcontinental lithospheric mantle, as suggested by Farmer et al. (2002) for Cenozoic potassic magmatism in the western United States.

More support for a model of lithosphere thinned by upwelling asthenosphere below the north-central Lut block comes from the tomographic imaging of the uppermost mantle velocity below the Iranian plateau. As documented by Hatzfeld and Molnar (2010), P and S wave tomography conducted on a regional scale indicate lower P and/or S-wave speeds in the uppermost mantle beneath central and eastern Iran than beneath the Zagros and adjacent Arabian platform. Low speeds and high attenuation are usually interpreted as implying relatively high temperatures. Moreover, the contrast between these regions is revealed to be sharp, with high wave speeds beneath the Zagros and lower speeds beneath the region to the northeast (Al-Lazki et al. 2004; Kaviani et al. 2007; Paul et al. 2010; Hatzfeld and Molnar 2010; Motaghi et

al. 2012). Low-speed and highly attenuating seismic waves suggest that today the mantle below the north-central Lut block is still relatively hot as would be the case if the mantle lithosphere is thin and hot asthenosphere had upwelled below this region since the collision of Arabai with Iran (Hatzfeld and Molnar 2010).

The last stage of volcanic activities (Neogene /Quaternary) include the alkali olivine basalts erupted mainly along the major faults that border the Lut block. This small low-volume of basaltic rocks have been formed by low but variable degrees of partial melting of EM-type mantle source (Saadat et al. 2010; Pang et al. 2012; Kheirkhah et al. 2015) produced by upwelling asthenosphere replacing the thinned lithospheric mantle (Fig. 12c). Deep strike-slip faulting might have played an important role in focusing the eruption of these low volume of mafic magmas, by generating localized extension and pull-apart basins (Keskin 2005; Cooper et al. 2002). In summary, the Neogene mafic rocks along the margins of the Lut block represent only the last manifestation of a much more extensive mid-Tertiary magmatic event.

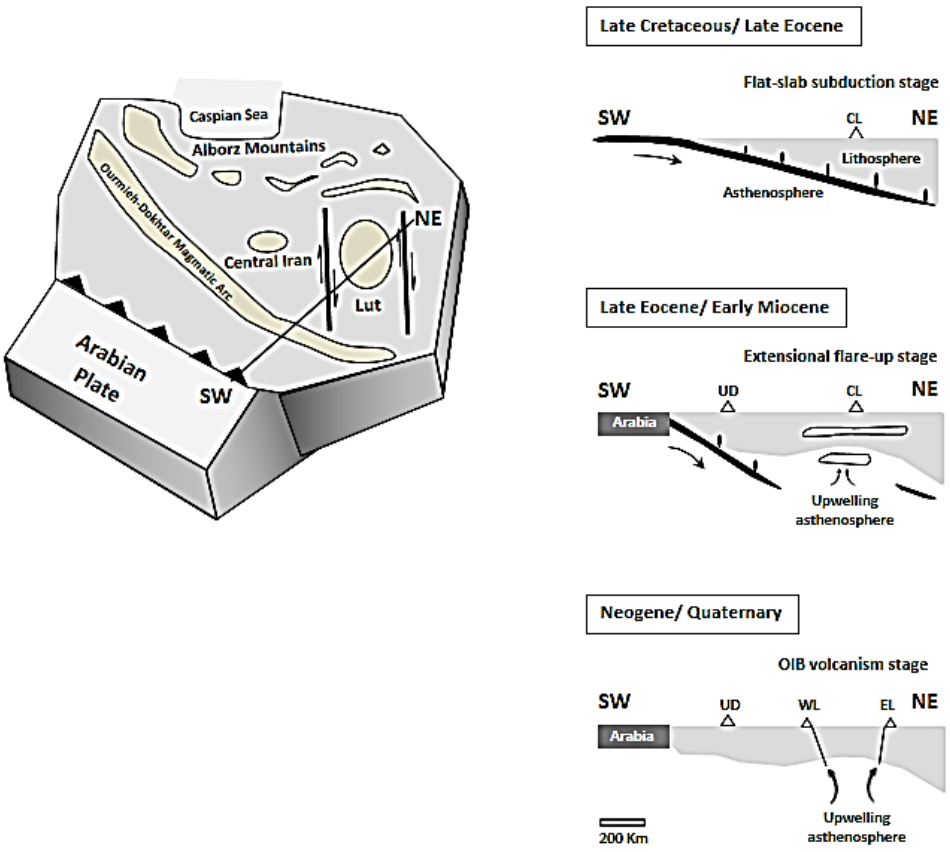

Fig. 12. Diagram, modified from Verdel (2009), summarizing the sequential development from Late Cretaceous/Late Eocene flat slab subduction stage, followed by a Late-Eocene/Early Miocene extentional flare-up stage as subduction geometry changes in response to the closure of Neotethys, and subsequent OIB-type Neogene/Quaternary magmatism along the margins of the Lut block. Abbreviations: UD-Urumieh-Dokhtar magmatic arc, CL-Central Lut, WL-Western Lut, EL-Eastern Lut.

6. Conclusion

The maximum volcanic activity within the north-central Lut block took place during Eocene time. This is consistent with the most extensive and intense volcanic activity in the central volcanic provinces of Iran (Stocklin 1974; Farhoudi 1978; Berberaian and King 1981). Paleogene basalts formed from both OIB-like asthenosphere and subcontinental lithosphere, which preserved chemical characteristics inherited from Mesozoic and early-Tertiary subduction associated with the collision of the Arabian with the Eurasian plate and closing of the Neotethys oceans which bounded the Lut block. From Eocene-early Oligocene to Neogene/Quaternary, there is a significant transition in composition and volume of volcanism, from mainly intermediate and felsic with calc-alkaline characteristic to mafic alkaline magmatism, with trace element compositions similar to those of oceanic island basalts (Figs. 5 and 10), limited spatially to the deep lithospheric structures along the margins of the Lut block (Saadat et al. 2010; Saadat and Stern 2012, 2014; Pang et al. 2012; Kheirkhah et al. 2015).

Acknowledgments

Financial support was provided by the Society of Economic Geology (SEG) and the Department of Geological Sciences at the University of Colorado. We thank E. Verplank with help obtaining the isotopic analysis, and J. Drexler for assistance with the microprobe analysis; Thanks also to Paul Boni for his help and advice in preparing the thin and polished thin section. We are grateful for M. Ghoorchi for help in preparing Figure 1 and F. Ghaemi, Fatemeh Noorian and Soroush Saadat for assistance in the field.

References:

Alavi M, Vaziri H, Seyed-Emami K, Lasemi Y (1997) The Triassic and associated rocks of the Nakhlak and Aghdarband areas in central and northeastern Iran as remnants of the southern Turanian active continental margin, *Bulletin Geological Society of America 109, 12: 1563–1575*

Al-Lazki A.I, Sandvol E, Seber D, Barazangi M, T.N, Mohamad R (2004) Pn tomographic imaging of mantle lid velocity and anisotropy at the junction of the Arabian, Eurasian, and African plates. *Geophysical Journal International 158: 1024-040*

Angiboust S, Agard P, De Hoog J.C.M, Omrani J, Plunder A (2013) Insights on deep, accretionary subduction processes from the Sistan ophiolitic melange, Eastern Iran, *Lithos 156–159: 139–158*

Arjmandzadeh R, Karimpour M.H, Mazaheri S.A, Santos J.F, Medina J.M and Homam S.M (2011) Two-sided asymmetric subduction; implications for tectonomagmatic and metallogenic evolution of the Lut Block, eastern Iran, *Iranian Journal of Economic Geology 3: 1-14 (in Persian)*

Bagheri S, Stampfli M.G, (2008) The Anarak, Jandaq and Posht-e-Badam metamorphic complexes in central Iran: New geological data, relationships and tectonic implications, *Tectonophysics 451: 123-155*

Baker J.A, Menzies M.A, Thirlwall, M.F, MacPherson C.G, (1997) Petrogenesis of Quaternary Intraplate Volcanism, Sana'a, Yemen: Implications for Plume-Lithosphere Interaction and Polybaric Melt Hybridization, *Journal of Petrology 38-10: 1359-1390*

Ballmer M.D, Van Hunen J, Ito G, Bianco T.A, Tacklye P.J (2009) Intraplate volcanism with complex age-distance patterns: a case for small-scale sublithospheric convection, *Geochemistry Geophysics Geosystems 10-6: 1-22*

Baumann A, Spies O, Lensch G (1982) Strontium isotopic composition of post-ophiolthic Tertiary volcanics between Kashmar, Sabzevar and Quchan NE Iran, *Neues Jahrbuch fur Geologie und Palaontologie Abhandlungen 160*

Berberian F, and Berberian, M (1981) Tectono-plutonic episodes in Iran, in Delany, F.M., ed., Zagros-Hindu Kush-Himalaya Geodynamic Evolution, *American Geophysical Union Geodynamics Series 3: 5–32*

Berberian M, King G.C.P (1981) Towards a paleogeography and tectonic evolution of Iran, *Canadian Journal of Earth Sciences 18-2: 210-265*

Berberian M, Soheili M (1973) Structural history of central Lut; consolidation of the supposed Lut block during the Earlt Kimmerian orogeny- a preliminary field note, *Geological Survey of Iran, internal report 17*

Berberian M, Jackson J.A, Qorashi M, Khatib M.M, Priestley K, Talebian M, Ghafuri-Ashtiani M (1999) The 1997 May 10 Zirkuh (Qa'enat) earthquake: faulting along the Sistan suture zone of eastern Iran, *Geophysics Journal International 136: 671-694*

Besse J, Torcq F, Gallet Y, Ricou L.E, Krystyn L, Saidi A (1998) Late Permian to Late Triassic palaeomagnetic data from Iran: constraints on the migration of the Iranian block through the Tethyan Ocean and initial destruction of Pangaea, *Geophysical Journal International 135: 77-92*

Bina M.M, Bucur I, Pre´vot M, Daly L, Cantagrel J.M (1986) Paleomagnetism, Petrology and Geochronology of Tertiary magmatic and sedimentary units from Iran, *Tectonophysics 121: 303-329*

Briggs P (1996) The determination of forty elements in geological materials by inductively coupled plasma-atomic, Bf Arbogast, *U.S. Geological Survey open file report 02-223-G: 77-94*

Bröcker M, Fotoohi Rad G.R, Burgess R, Theunissen S, Paderin I, Rodionov N, Salimi Z (2013) New age constraints for the geodynamic evolution of the Sistan Suture Zone, eastern Iran, *Lithos 170–171: 17–34*

Camp V.E, Griffis R.J (1982) Character, genesis and tectonic setting of igneous rocks in the Sistan suture zone, eastern Iran, *Lithos 15: 221-239*

Carlson R.W, Hart, W.K (1987) Crustal genesis on the orogenic plateau, *Journal of Geophysical Research 92: 6191-6206*

Chiu H.Y, Chung S.L, Zarrinkoub M.H, Mohammadi S.S, Khatib M.M, Iizuka Y (2013) Zircon U-Pb age constraints from Iran on the magmatic evolution related to Neotethyan subduction and Zagros orogeny, *Lithos 162–163: 70–87*

Class C, Goldstein S. L (1997) Plume–lithosphere interactions in the ocean basins: constraints from the source mineralogy, *Earth and Planetary Science Letters 150: 245-260*

Conrad G, Montignary R, Thuizat R and Westphal M (1981) Tertiary and Quaternary geodynamics of southern Lut (Iran) as deduced from palaeomagnetic, isotopic and structural data, *Tectonophysics 75: 11-17*

Cooper K.M, Reid M.R, Dunbar N.W, and McIntosh W.C (2002) Origin of mafic magmas beneath northwestern Tibet: Constraints from ^{230}Th-^{238}U Disequilibria, *Geochemistry Geophysics Geosystems 3-11: 1-23*

Cox K.G, Bell J.D, Pankhurst R.J (1979) The Interpretation of Igneous Rocks, *George Allen and Unwin, London: 445*

Davoudzadeh M, Schmidt K (1984) A review of the Mesozoic paleogeography and paleotectonic evolution of Iran, *Neues Jahrbuch für Geologie und Paläontologie 168: 182-207*

Davoudzadeh M (1997) *Encyclopedia of European and Asian regional geology: 384-405*

Delaloye M, Desmons J (1980) Ophiolites and mélange terranes in Iran: A geochronological study and its paleotectonic implications, *Tectonophysics 68: 83-111*

Delavari M, Amini S, Saccani E, Beccaluva L (2009) Geochemistry and petrology of mantle peridotites from the Nehbandan ophiolitic complex, Eastern Iran, *Journal of Applied Sciences 9: 2671–2687*

Dercourt J, Zonenshain L.P, Ricou L. E, Kazmin V.G, Le Pichon X, Knipper A.L, Grandjacquet C, Sbortshikov I.M, Geyssant J, Lepvrier C, Pechersky D.H, Boulin J, Sibuet J.C, Savostin L.A, Sorokhtin O, Westphal M, Bazhenov M.L, Lauer J.P, Biju-Duval B (1986) Geological evolution of the Tethys belt from the Atlantic to the Pamirs since the Lias. *Tectonophys 123: 241-315*

Dercourt J, L.E, R, Vrielynck B (1993) Atlas Tethys Paleoenvironmental Maps, *Gauthier-Villars, Paris*

Esmaiely D, Nédéléc A, Valizadeh M.V, Moore F, Cotton J (2005) Petrology of the Jurrasic Shah-Kuh granite, eastern Iran, with reference to tin mineralization, *Journal of Applied Sciences 25: 961-980*

Fakhari M.D, Axen G.J. Horton B.K, Hassanzadeh J, Amini A (2008) Revised age of proximal deposits in the Zagros foreland basin and implications for Cenozoic evolution of the High Zagros, *Tectonophysics 451 (1-4): 170-185*

Farhoudi G (1978) A comparison of Zagros geology to island arcs, *Journal of Geology 86: 323-334*

Farmer G.L, Broxton E.D, Warren R.G, Pickthorn W (1991) Nd, Sr, and O isotopic variations in metaluminous ash flow tuffs and related volcanic rocks at Timber Mountain/Oasis Valley Caldera, Complex, SW Nevada: implication for the origin and evolution of large-volume silicic magma bodies, *Contributions to Mineralogy and Petrology 109: 53-68*

Farmer G.L, Fornash K.F (2009) Geochemical Evidence for Early to Mid-Cenozoic "Flat-Slab" Subduction Beneath the Western North American Interior, *American Geophysical Union, Fall Meeting, abstract #: V41B-2186*

Farmer G.L, Glazner A.F, Manley C.R (2002) Did lithospheric delamination trigger late Cenozoic potassic volcanism in the southern Sierra Nevada, California, *Bulletin Geological Society of America 114-6: 754-768*

Fotoohi Rad G.R, Droop G.T.R, Amini, T.S, Moazzen M (2005) Eclogites and blueschists of the Sistan Suture Zone, eastern Iran: A comparison of P–T histories from a subduction melange, Lithos 84: 1- 24

Gerlach D, Frey F.A, Moreno-Roa H (1988) Recent volcanism in the Puheyue-Cordon Caulle region, southern Andes, Chile (40.5°S); Petrogenesis of evolved lavas, *Journal of Petrology 29: 332-382*

Ghorbani G (1997) Petrogenetic studies of Eastern Iran Quaternary Basalts (Khorasan), *Shahid Beheshti University, Tehran, Iran, Master Thesis: 192 (in Persian)*

Golonka J (2000) Geodynamic evolution of the south Caspian Basin, *AAPG's Inaugural Regional International Conference, Istanbul, Turkey: 40- 45*

Golonka J (2004) Plate tectonic evolution of the southern margin of Eurasia in the Mesozoic and Cenozoic, *Tectonophysics 381: 235- 273*

Golonka J, Ross M.I, Scotese C.R (1994) Phanerozoic paleogeographic and paleoclimatic modeling maps. In: Embry, A.F., Beauchamp, B., Glass, D.J. (Eds.), Pangea, *Global Environmental Resources 17: 1- 47*

Haghipour A (1981) Precambrian in central Iran: lithostratigraphy, structural history and petrology, *Iranian Petroleum Institute Bulletin 81:1-17*

Hart S.R (1984) A large-scale isotope anomaly in the Southern Hemisphere mantle, *Nature 30: 753–757*

Hart S.R (1988) Heterogeneous mantle domains: signatures, genesis and mixing chronologies, *Earth and Planet Science Letters 90: 273–296*

Hassanzadeh J, Stockli D.F, Horton B.K, Axen G.J, Stockli L.D, Grove, M, Schmitt A.K, Douglas Walker J (2008) U-Pb zircon geochronology of late Neoproterozoic-Early Cambrian granitoids in Iran: Implications for paleogeography, magmatism, and exhumation history of Iranian basement, *Tectonophysics 451: 71-96*

Hatzfeld D, Molnar P (2010) Comparisons of the kinematics and deep structures of the Zagros and Himalaya and of the Iranian and Tibetan Plateaus, and geodynamic implications. *Reviews of Geophysics 48, RG2005: 1-48*

Hofmann A.W (1997) Mantle geochemistry: the message from oceanic magmatism, *Nature 385: 219-229*

Hofmann A.W, Jochum K.P, Seufert M, White W.M (1986) Nb and Pb in oceanic basalts: new constraints on mantle evolution, *Earth and Planetary Science Letters 79: 33-45*

Horton B.K, Hassanzadeh J, Stockli D.F, Axen G.J, Gillisa R.J, Guesta B, Aminic A, Fakharia M.D, Zamanzadehc S.M, Grovea M (2008) Detrital zircon provenance of Neoproterozoic to Cenozoic deposits in Iran: Implications for chronostratigraphy and collisional tectonics, *Tectonophysics 451: 97-122*

Jackson J (1992) Partitioning of strike-slip an convergent motion between Eurasia and Arabia in eastern Turkey and Arabia, *Journal of Geophysical Research 97: 12479-12741*

Jung D, Keller J, Khorasani R, Marcks C, Baumann A, Horn P (1984) Petrology of the Tertiary magmatic activity in the northern Lut area, east Iran, *Neues Jahrbuch fur Geologie und Palaontologie 160: 417-467*

Karimpour M.H, Stern C.R, Farmer G.L, Saadat S, Malekzadeh Shafaroudi A (2011) Review of Age, Rb-Sr Geochemistry and Petrogenesis of Jurassic to Quaternary Igneous rocks in Lut Block, Eastern Iran *Geopersia 1: 19-36*

Karimpour M.H, Zaw K, Huston D.L (2005) S-C-O Isotopes, fluid Inclusion, microthermometry, and the genesis of ore bearing fluids at Qaleh-Zari Fe-Oxide Cu-Au-Ag mine, Iran, *Journal of Sciences, Islamic Republic of Iran 16-2: 153-168*

Kaviani A, Paul A, Bourova E, Hatzfeld D, Pedersen H, Mokhtari M (2007) A strong seismic velocity contrast in the shallow mantle across the Zagros collision zone-Iran, *Geophysical Journal International 171: 399-410*

Kazmin V.G, Lobkovsky L.I, Tikhonova N.F (2010) Late Cretaceous–Paleogene Deepwater Basin of North Afghanistan and the Central Pamirs: Issue of Hindu Kush Earthquakes, *Geotectonics 44-2:127-138*

Kazmin V.G, Sbortshikov I.M, Ricou L-E, Zonenshain L.P, Boulin J, Knipper A.L (1986) Volcanic belts as markers of the Mesozoic-Cenozoic active margin of Eurasia, *Tectonophysics 123: 123-152*

Keskin M (2005) Domal uplift and volcanism in a collision zone without a mantle plume: Evidence from Eastern Anatolia, *http://www.MantlePlumes.org*

Kheirkhah M, Neill I, Allen M.B (2015) Petrogenesis of OIB-like basaltic volcanic rocks in a continental collision zone: Late Cenozoic magmatism of Eastern Iran, *Journal of Asian Earth Sciences 106: 19–33*

Kopp M.L (1997) Lateral escape structures in the Alpine-Himalayan collision belt , *Russian Academy of Sciences Transactions 506:1-314 (In Russian)*

Leeman W.P, Hawkesworth C.J (1986) Open magmatic systems, some isotopic and trace element constraints, *Journal of Geophysical Research 91: 5901-5912*

Malekzadeh A (2009) Geology, mineralization, alteration, geochemistry, microthermometry, isotope studies and determining the mineralization source of Khoopic and Maherabad exploration areas, *Ph.D thesis, Ferdowsi University of Mashhad, Iran*

McCall G.J.H (1985) *Area report, East Iran Project, Area No. 1:57*

McDonough W.F (1990) Constrains on the composition of the continental lithospheric mantle, *Earth and Planetary Science Letters 101:1-18*

Middlemost E.A.K (1975) The basalt clan, *Earth Science Review 11: 337-364*

Motaghi K, Tatar M, Shomali Z.H, Kaviani A, Priestley K (2012) High resolution image of uppermost mantle beneath NE Iran continental collision zone, *Physics of the Earth and Planetary Interiors 208–209: 38–49*

Myashiro A (1978) Nature of Alkalic volcanic rock series, *Contributions to Mineralogy and Petrology 66: 91-104*

Nadimi, A (2007) Evolution of central Iranian basement, *Gondwana Research 12-3: 324-333*

Pang KN, Chung SL, Zarrinkoub, M.H, Mohammadi, S.S, Yang, HM, Chu, CH, Lee, HY, Lo, CH (2012) Age, geochemical characteristics and petrogenesis of Late Cenozoic intraplate alkali basalts in the Lut-Sistan region, eastern Iran, *Chemical Geology 306–307: 40–53*

Pang KN, Chung SL, Zarrinkoub M.H, Khatib, M.M, Mohammadi S.S, Chiu, HY, Chu CH, Lee HY, Lo CH (2013) Eocene–Oligocene post-collisional magmatism in the Lut–Sistan region, eastern Iran: Magma genesis and tectonic implications. *Lithos 180–181:234–251*

Paul A, Hatzfeld D, Kaviani A, Tatar M, Péquegnat C (2010) Seismic imaging of the lithospheric structure of the Zagros mountain belt, Iran, *Geological Society of London Special Publications 330: 5-18*

Ramezani J, Tucker R.D (2003) The Saghand region, central Iran: U-Pb geochronology, petrogenesis and implications for Gondwana tectonics, *American Journal of Science 303: 622-665*

Reed S.J.B (1996) Electron Microscope Analysis and Scanning Electron Microscopy in Geology, *Cambridge University Press: 201*

Richards J, Spell T, Rameh E, Razique A, Fletcher, T (2012) High Sr/Y Magmas Reflect Arc Maturity, High Magmatic Water Content, and Porphyry Cu ± Mo ± Au Potential: Examples from the Tethyan Arcs of Central and Eastern Iran and Western Pakistan, *Economic Geology 107: 295-332*

Rudnick R.L, Fountain D.M (1995) Nature and composition of the continental crust: a lower crustal perspective, *Geophysics 33: 267-309*

Saadat S, Stern C.R (2011) Petrochemistry and genesis of olivine basalts from small monogenetic parasitic cones of Bazman stratovolcano, Makran arc, southeastern Iran, *Lithos 125: 607-619*

Saadat S, Stern C.R (2012) Petrochemistry of a xenolith-bearing Neogene alkali olivine basalt from northeastern Iran, *Journal of Volcanology Geothermal Research 225–226: 13–29*

Saadat S, Stern C.R (2014) Petrochemistry of ultrapotassic tephrites and associated cognate plutonic xenoliths from late Quaternary Qa'le Hasan Ali maars, central Iran, *Journal of Asian Earth Sciences 89: 108-122*

Saadat S, Karimpour M.H, Stern C.R (2010) Petrochemical characteristics of Neogene and Quaternary alkali olivine basalts from the western margin of the Lut block, eastern Iran, *Iranian Journal of Earth Sciences 2: 87-106*

Saccani E, Delavari M, Beccaluva L, AminiSadr A (2010) Petrological and geochemical constraints on the origin of the Nehbandan ophiolitic complex (eastern Iran): Implication for the evolution of the Sistan Ocean, *Lithos 117: 209-228*

Saidi A, Brunet M.F, Ricou L.E (1997) Continental accretion of the Iran block to Eurasia as seen from Late Paleozoic to Early Cretaceous subsidence curves, *Geodynamic Acta 10: 189-208*

Samani B, Zhuyi C, Xuetao G, Chuan T (1994) Geochemistry of Quaternary Olivine Basalts From the Lut Block, Eastern Iran, *Geodynamic Acta 3-10: 40-63*

Savostin L.A, Sibuet J.-C, Zonenshain L.P, Le Pichon X, Roulet M.-J (1986) Kinematic evolution of the Tethys belt from the Atlantic Ocean to the Pamirs since the Triassic, *Tectonophysics 123: 1-35*

Sengör A.M.C, Natalin B.A (1996) Paleotectonics of Asia: fragment of a synthesis. In: Yin, An, Harrison, T.M. (Eds.), *The Tectonic Evolution of Asia: 486- 640*

Sengör A.M.C (1990) A new model for the late Paleozoic-Mesozoic tectonic evolution of Iran and implications for Oman, *Geological Society of London Special Publication 49: 797-831*

Shabanian E, Acocella V, Gioncada A, Ghasemi H, Bellier O (2012) Structural control on volcanism in intraplate post collisional settings: Late Cenozoic to Quaternary examples of Iran and eastern Turkey. Tectonics 31, TC3013, 1-25

Shahabpour J (2005) Tectonic evolution of the orogenic belt in the region located between Kerman and Neyriz, *Journal of Asian Earth Sciences 24: 405-417*

Shojaat B, Hassanipak A.A, Mobasher K, Ghazi A.M (2003) Petrology, geochemistry and tectonics of the Sabzevar ophiolite, North Central Iran, *Journal of Asian Earth Sciences 21: 1053-1067*

Sims K.W.W, DePaolo D.J (1997) Inferences about mantle magma sources from incompatible element concentration ratios in oceanic basalts, *Geochimica et Cosmochimica Acta 61-4: 765-784*

Soffel G, Davoudzadeh M, Rolf C, Schmidt S (1996) New paleomagnetic data from central Iran and a Triassic reconstruction, *Geologische Rundschau-85: 293-302*

Soffel H.C, Forster H.G (1980) Apparent polar wander path of central Iran and its geotectonic interpretation, *Journal of Geomagnetism and Geoelectricity-32: 117-135*

Spies O, Lensch G, Mihem A (1983) Chemistry of the post-ophiolitic Tertiary volcanism between Sabzevar and Quchan/NE Iran. Geodinamic Project (Geotraverse) in Iran, final report, *Geological Survey of Iran: 53*

Stöcklin J, Eftekhamejad J, Hoshmandzadeh A (1971) Initial investigation of central Lut block, eastern Iran, *Geological Survey of Iran: 22*

Stöcklin J (1974) Possible ancient continental margins in Iran, in Geology of Continental Margins, *Springer-Verlag, New York edited by C. Burk and C. Drake: 873-877*

Takin M (1972) Iranian geology and continental drift in the Middle East, *Nature 235: 147-150*

Tarkian M, Lotfi M, Baumann A (1984) Magmatic copper and lead zinc ore deposits in the Central Lut, East Iran, *Neues Jahrbuch fuer Geologie und Paläontologie, Abhandlungen 168: 497- 523*

Tarkian M, Bock W.D, Neumann M (1983) Geology and mineralogy of the Cu−Ni−Co−U ore deposits at Talmessi and Meeskani, central Iran, *Contributions of Mineralogy and Petrology 32-2-3: 111-133*

Taylor S.R, McLennan S.M (1985) The continental crust: Its composition and evolution, *Blackwell Scientific Publications: 312*

Thirlwall M.F, J, U.B.G, Jenkins C (1994) Interaction between continental lithosphere and the Iceland Plume Sr-Nd-Pb isotope geochemistry of Tertiary basalts, NE Greenland, *Journal of Petrology 35: 839-879*

Thompson R.N, Morrison M.A, Dickin A.P, Hendry G.L (1983) Conti)nental flood basalts. Arachnids rule OK? in "Continental basalts and mantle xenoliths." Nantwich, UK: Shiva: 158-185

Van Calsteren N.B.W, Harris P.W.C, Hawkesworth C.J, Menzies M.A, Rogers N.W (1986) Xenoliths from southern Africa: a perspective on the lower crust, *Geological Society of London Special Publications 24: 351-362*

Verdel C (2009) I. Cenozoic geology of Iran: An integrated study of extensional tectonics and related volcanism, II. Ediacaran strtigraphy of the north American cordillera: new observation from eastern California and northern Utah, *California Institute of Technology, Pasadena, California: 287*

Vosughi Abedini M (1997) Petrologic and tectonomagmatic aspects of Cenozoic basalts in Iran (Khorasan), *Earth Science Journal 23-24: 16-30*

Walker R.T, Gans P, Allen M.B, Jackson J, Khatib M, Marsh N, Zarrinkoub M (2009) Late Cenozoic volcanism and rates of active faulting in eastern Iran, *Geophysical Journal International 177: 783-805*

Weaver B.L, Tarney J (1984) Empirical approach to estimating the composition of the continental crust, *Nature 310: 575-577*

Wedepohl K.H (1994) The composition of the continental crust(abstract), *Mineralogical Magazine 58: 359-360*

Wensink H, Varekamp J.C (1980) Paleomagnetism of basalt from Alborz: Iran part of Asia in the Cretaceous, *Tectonophysics 68: 113-129*

Wensink H, (1979) The implications of some paleomagnetic data from Iran for its structural history, *Geologie en Mijnbouw 58: 175-185*

Wensink H (1982) Tectonic inferences of paleomagnetic data from Mesozoic formations in central Iran, *Journal of Geophysics 51: 12-23*

Westphal M, Bazhenov M.L, Lauer J.P, Pechersky D.M, Sibuet J.C (1986). Paleomagnetic implications on the evolution of the Tethys belt from the Atlantic ocean to the Pamirs since the Triassic, *Tectonophysics 123: 37-82*

Zarrinkoub M.H, Pang K.N, Chung S.L, Khatib M.M, Mohammadi S.S, Chiu H.Y, Lee H.Y (2012). Zircon U–Pb ages and geochemical constraints on the origin of the Birjand ophiolite, eastern Iran. *Lithos 154: 392–405*

Zarrinkoub M.H, Chung S.L, Mohhamadi S.S, Khatib M.M (2008) Age dating, petrography and geochemistry of Fanoud volcanic rocks (South east of Birjand, Iran), *16th Iranian Society of Crystallography and Mineralogy, Iran*